

Electronic Supplementary Material (ESI) for Chemical Science.

This journal is © The Royal Society of Chemistry 2025

Supporting Information

Inter-Cluster-Linker-Absence-Enabled Sub-Ångstrom Pore Modulation in Metal-Organic Framework for Multi-Scenario CO₂ Capture

Jia-Wen Wang, Shu-Cong Fan, Wenyu Yuan, Ying Wang and Quan-Guo Zhai*

Key Laboratory of Applied Surface and Colloid Chemistry (MOE), Key Laboratory of Macromolecular Science of Shaanxi Province, School of Chemistry & Chemical Engineering, Shaanxi Normal University, Xi'an, Shaanxi, 710062, China.

*Corresponding author. Email: zhaiqg@snnu.edu.cn

Experimental Section

General materials and methods. All reagents were purchased commercially and used without further purification. The as-synthesized material was characterized by powder X-ray diffraction (PXRD) and single-crystal X-ray diffraction measurements. The simulated powder pattern was calculated using single-crystal X-ray diffraction data and processed by the Mercury 2.3 program provided by the Cambridge Crystallographic Data Centre. Thermogravimetric analyses (TGA) were performed on HCT-1 thermal analyzer at a heating rate of $10\text{ }^{\circ}\text{C min}^{-1}$ up to $600\text{ }^{\circ}\text{C}$ with an N_2 flow rate of 2 mL min^{-1} . Field emission scanning electron microscopy (FE-SEM) analyses were tested on a SU8220 spectrometer (Hitachi Co. Ltd, Japan) with 10 kV . Samples were outgassed in vacuum at $120\text{ }^{\circ}\text{C}$ for 5.5 h to remove all guest molecules prior to the test. The CO_2 temperature programmed desorption (CO_2 -TPD) curves of SNNU-98-Cd/Cu were conducted on an AutoChem II 2920VG catalytic characterization system.

Caution. Tetrazole ligand is potentially explosive. Only small amounts of tetrazole should be prepared and handled with care.

Synthesis of SNNU-98-Cd. SNNU-98-Cd with high crystallinity was successfully synthesized based on a modification of previously reported method.¹ A mixture of cadmium nitrate tetrahydrate ($\text{Cd}(\text{NO}_3)_2 \cdot 4\text{H}_2\text{O}$) (76 mg, 0.25 mmol) and tetrazole (TAZ) (35 mg, 0.5 mmol) was dissolved into 5 mL water and 1 mL CH_3CN in a 25 mL sealed Teflon-lined stainless-steel vessel. Then the mixture was under stirring for 30 min at room temperature and then heated at $170\text{ }^{\circ}\text{C}$ for 3 days. After cooling down to room temperature, transparent columnar crystals can be obtained without any washing (73% yield based on Cd).

Synthesis of SNNU-98-Cu. A mixture of copper nitrate hydrate ($\text{Cu}(\text{NO}_3)_2 \cdot 3\text{H}_2\text{O}$) (121 mg, 0.5 mmol), TAZ (50 mg, 0.7 mmol) was dissolved into 8 mL water in a 25 mL sealed Teflon-lined stainless-steel vessel. Then the mixture was under stirring for 30 min at room temperature and then heated at $150\text{ }^{\circ}\text{C}$ for 3 days. After cooling down to room temperature, blue powder can be obtained without any washing (86% yield based on Cu).

Large-scale synthesis of SNNU-98-Cu. A mixture of copper nitrate hydrate ($\text{Cu}(\text{NO}_3)_2 \cdot 3\text{H}_2\text{O}$) (19.36 g), TAZ (8 g) was dissolved into 640 mL water in a 1000ml round-bottomed flask. Then the mixture was under stirring for 10 min at room temperature and then reflux heated at $150\text{ }^{\circ}\text{C}$ for 30 min. After cooling down to room temperature, blue powder can be obtained without any washing (85% yield based on Cu).

Single-crystal X-ray diffraction measurements. Crystallographic data for the SNNU-98-Cd was carried out on XtaLABmini II single crystal diffractometer with Mo K α radiation ($\lambda = 0.71073\text{ \AA}$) at 200 K. Using Olex2, the structures were solved with the ShelXT structure solution program using intrinsic phasing and refined by full matrix least-squares methods with the ShelXL program package. The structure was solved by direct methods and refined using ShelXT. SQUEEZE routine in PLATON software package was employed to fix solvents in lattice pores. Crystal data as well as details of data collection and refinements are summarized in Tables S2 (CCDC: 2416690).

Powder X-ray diffraction (PXRD) characterization. Powder X-ray diffraction experiments were performed on a MiniFlex 600 diffractometer, which was operating at 40 kV and 15 mA (Cu K α radiation, $\lambda = 1.5406\text{ \AA}$). The data collection was performed at room temperature with an angle range from 5° to 50° with a step size of $\approx 0.020^{\circ}$. The simulated powder pattern was obtained from the single crystal data.

Thermogravimetric (TG) measurements. The thermal gravimetric analysis was performed on HCT-1 thermogravimetric analyzer at a heating rate of 10 °C min⁻¹ up to 600 °C with N₂ flow rate of 2 mL min⁻¹. The sample holders were alumina crucibles and the amount of each sample used during the tests was 5 (± 2) mg.

Stability tests. One batch of MOF samples was immersed in pH = 1-14 or 1-3 M HCl solution for PXRD and 195 K CO₂ adsorption experiments at 24 hours, 1 week, 1 month, 2 months and even 6 months, respectively. The pH was adjusted with concentrated hydrochloric acid solution or sodium hydroxide.

Single gas adsorption measurements. Gas adsorption-desorption isotherms for SNNU-98-Cd/Cu were measured with a Micromeritics 3-Flex surface-area and pore-size analyzer up to 1 atm of gas pressure by the static volumetric method. The as-synthesized samples were immersed in methanol for 3 days (the solution was refreshed three times during each day) and then degassed under vacuum at 120 °C for 5.5 hours. For all of the samples, CO₂, CH₄, and N₂ adsorption isotherms were tested at 273, 283, and 298 K using 50-100 mg of sample, respectively. The Brunauer–Emmett–Teller (BET) surface area of the sample was calculated from the 195 K CO₂ adsorption isotherm by the BET equation. The low temperature at 195 K was controlled by a Dewar filled with dry ice/acetone mixtures.

Calculation of adsorption selectivity. Used the gas adsorption isotherms for all of the samples. The selectivity was calculated by ideal adsorbed solution theory (IAST). The Langmuir–Freundlich (LF) equation was employed to fit the gas adsorption isotherms over the entire pressure range. Based on the above equation parameters of pure gas adsorption, the IAST model was used to investigate the separation of CO₂/N₂, CO₂/CH₄, and CH₄/N₂ at different temperatures in component SNNU-98-Cd/Cu and the adsorption selectivity is defined by

$$S_{A/B} = \frac{x_A / y_A}{x_B / y_B}$$

where x_i and y_i are the mole fractions of component i ($i = A, B$) in the adsorbed and bulk phases, respectively.

Calculation of adsorption enthalpy Q_{st}. The isosteric heat of adsorption for all the gases were calculated using the isotherms at 273, 283, and 298 K by the virial model. To extract the coverage-dependent isosteric heat of adsorption, the data were modeled with a virial-type expression composed of parameters a_i and b_i that are independent of temperature:

$$\ln P = \ln N + \frac{1}{T} \sum_{i=0}^m a_i N^i + \sum_{i=0}^n b_i N^i$$

$$Q_{st} = -R \sum_{i=0}^m a_i N^i$$

where P is pressure expressed in Pa, N is the amount adsorbed (or uptake) in mmol g⁻¹, T is the temperature in K, and m and n represent the number of coefficients required to adequately describe the isotherms, and a_i and b_j are virial coefficients. Q_{st} (kJ mol⁻¹) is the isosteric heat of adsorption at a specific surface loading of adsorbate, R (kJ·mol⁻¹·K⁻¹) is the universal gas constant.

Breakthrough separation experiments. The CO₂/N₂, CO₂/CH₄, CH₄/N₂, CO₂/CH₄/N₂ and CO₂/CH₄/N₂/CO/H₂ breakthrough experiments for SNNU-98-Cd/Cu were performed in a self-assemble equipment. Activated MOF samples of 0.5-1.0 g (0.8560 g for SNNU-98-Cd and 1.0588 g for SNNU-98-Cu) were loaded into a stainless-steel column with an internal diameter of about 3.88 mm and both ends were sealed with absorbent cotton. The

column was placed in a circulating catheter sleeve connected to a thermostatic bath (temperature range from 273 K to 298 K). The flow and pressure of the mixed gas are controlled by the pressure control valve and the mass flow controller, respectively. The outlet effluent was continuously monitored using mass spectrometry (Hiden, HPR-20). Before the start of each breakthrough experiment, the sample column was purged with He flow (30 mL min⁻¹) for 3-5 hours to further activate the sample.

In addition, breakthrough experiments at 98% humidity with CO₂/N₂ (15/85, v/v) were tested by passing the gas into water in a closed container and flowing out through a bulge. The CO₂/N₂ separation experiment at 50% humidity was tested on a MIX100_SMPPRO Instruments (Advanced Measurement Instruments, Inc.) with He gas passed as carrier gas.

Separation Factor and Dynamic Capacity: Based on the mass balance, the amount of gas adsorbed i (q_i) is calculated from the breakthrough curve using the following:

$$q_i = \frac{C_i V}{22.4 \times m} \times \int_0^t \left(1 - \frac{F}{F_0}\right) dt$$

Where q_i is the equilibrium adsorption capacity of gas i (mmol g⁻¹), C_i is the feed gas concentration, V is the volumetric feed flow rate (cm³ min⁻¹), t is the adsorption time (min), F₀ and F are the inlet and outlet gas molar flow rates, respectively, and m is the mass of the adsorbent (g).

Grand Canonical Monte Carlo (GCMC) simulations. The simulations were done in the sorption module of Material Studio 8.0. The GCMC method was used to predict the distribution of electron cloud density and adsorption sites for guest molecules in SNNU-98-Cd/Cu. Before the simulations, the guest gas molecules and the structures were optimized by the forcite module. And the unit cells of 2 × 2 × 1 supercell were used as the simulation boxes. A total of 1 × 10⁷ steps was used for equilibration, and 1 × 10⁷ production steps were used to calculate the ensemble average of gas adsorption sites. The cutoff radius used for the Lennard-Jones interactions was 18.5 Å. The long-range electrostatic interactions were treated using the Ewald summation technique. Obtaining an accessible Connolly surface for SNNU-98-Cd/Cu by using the Connolly radius of 1.8 Å and the Grid interval of 0.15 Å.

Results and discussion

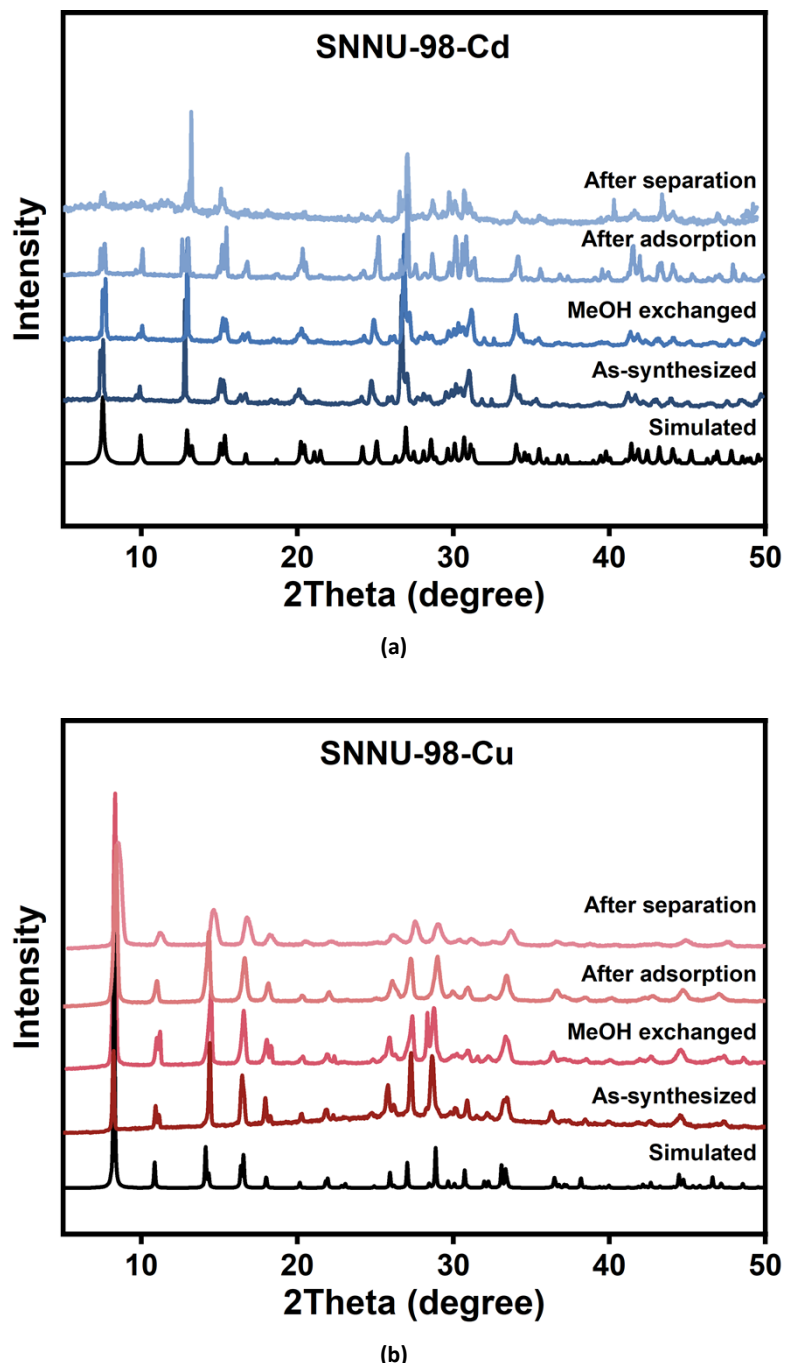


Figure S1. The PXRD patterns of SNNU-98-Cd (a) and SNNU-98-Cu (b) (as-synthesized, after MeOH exchange, after gas adsorption, and after breakthrough experiments).

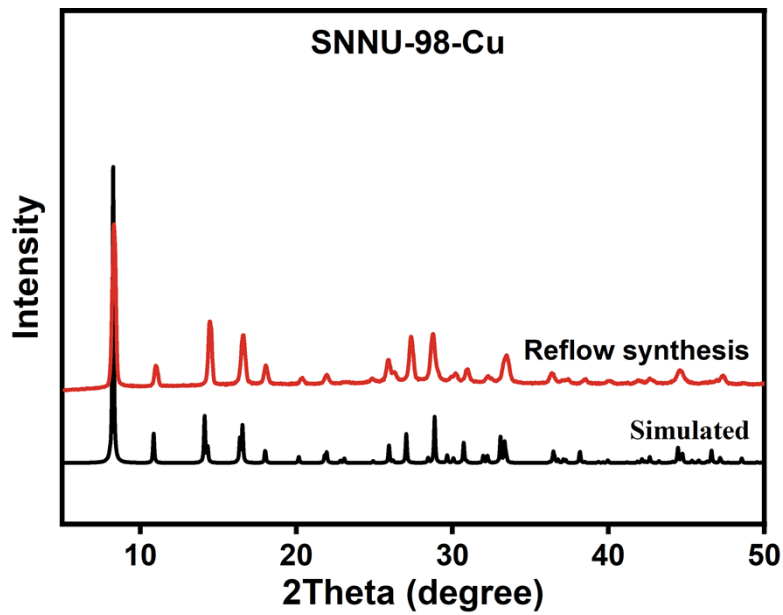


Figure S2. The PXRD patterns of SNNU-98-Cu synthesized by reflux on a large scale.

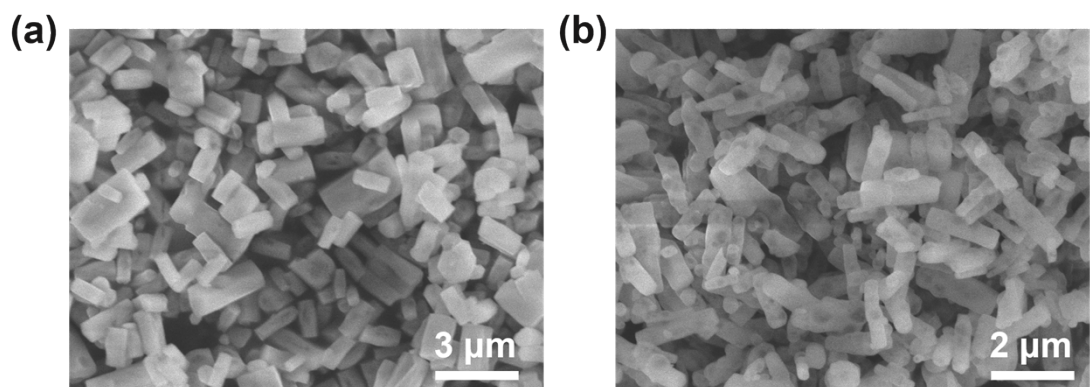
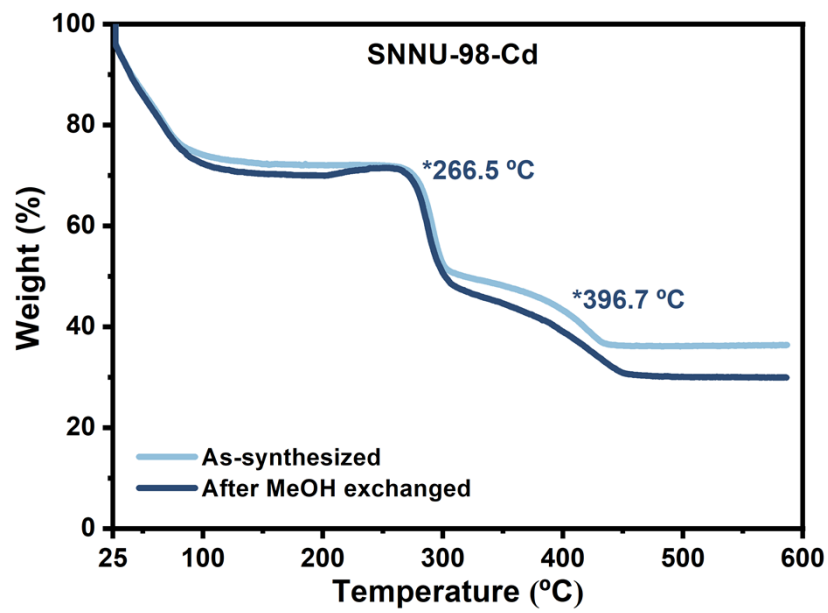
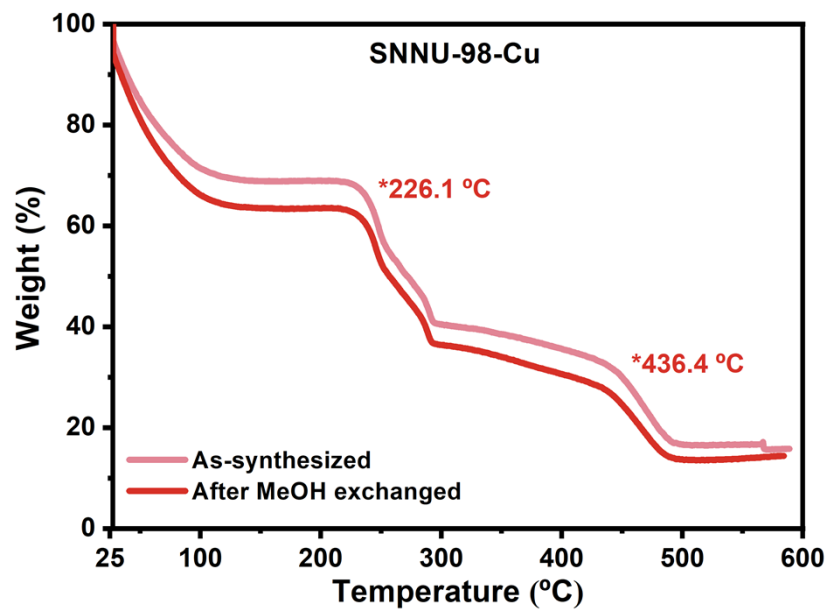


Figure S3. Scanning electron microscopy (SEM) images of **SNNU-98-Cu** synthesized by (a) hydrothermal and (b) reflux methods.



(a)



(b)

Figure S4. Thermogravimetric analysis (TGA) curves of the as-synthesized and activated samples of SNNU-98-Cd/Cu.

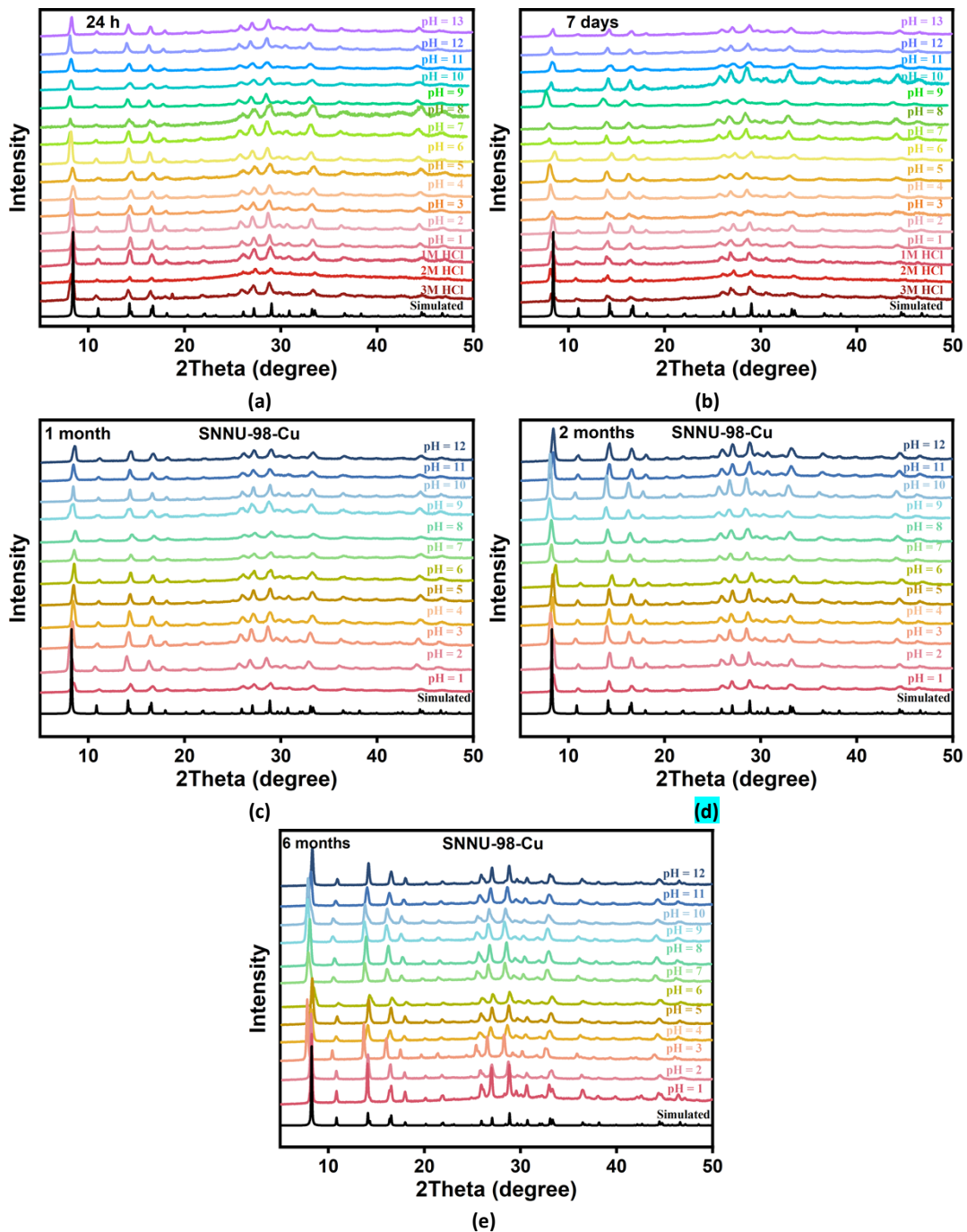


Figure S5. The PXRD patterns of SNNU-98-Cu immersed in pH = 1-13 and 1-3 M HCl solution for 24 hours (a), 7 days (b), 1 month (c), 2 months (d) and 6 months (e).

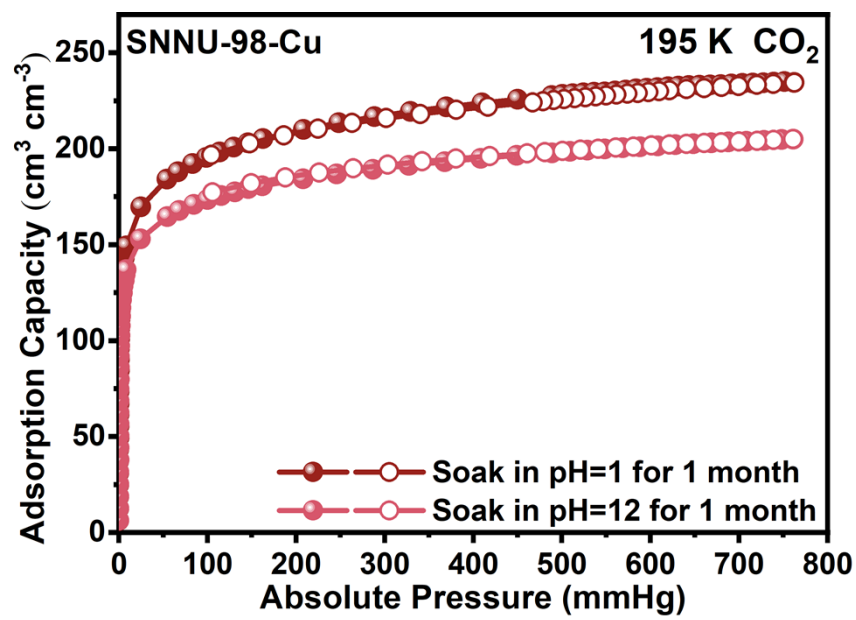


Figure S6. The 195 K CO₂ adsorption curves and the corresponding pore size distribution of **SNNU-98-Cu** after immersed in pH = 1-12 solution for 1 month.

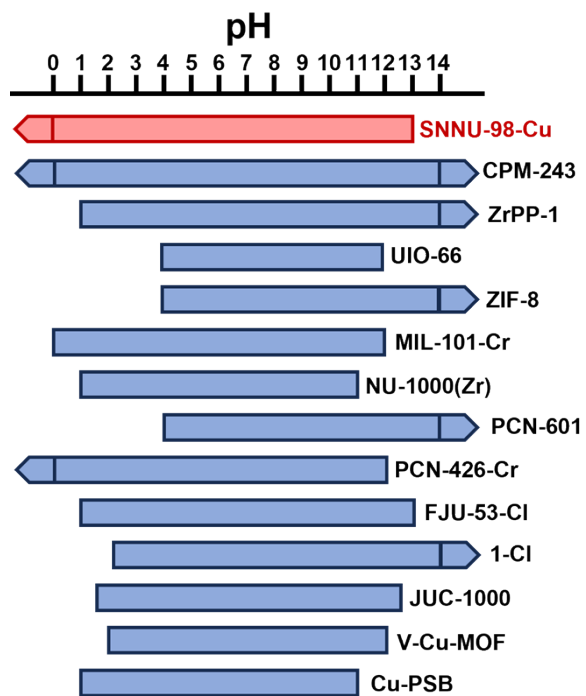


Figure S7. Stability comparison of top-level robust MOFs (the arrow indicates stability under pH < 0 or pH > 14).

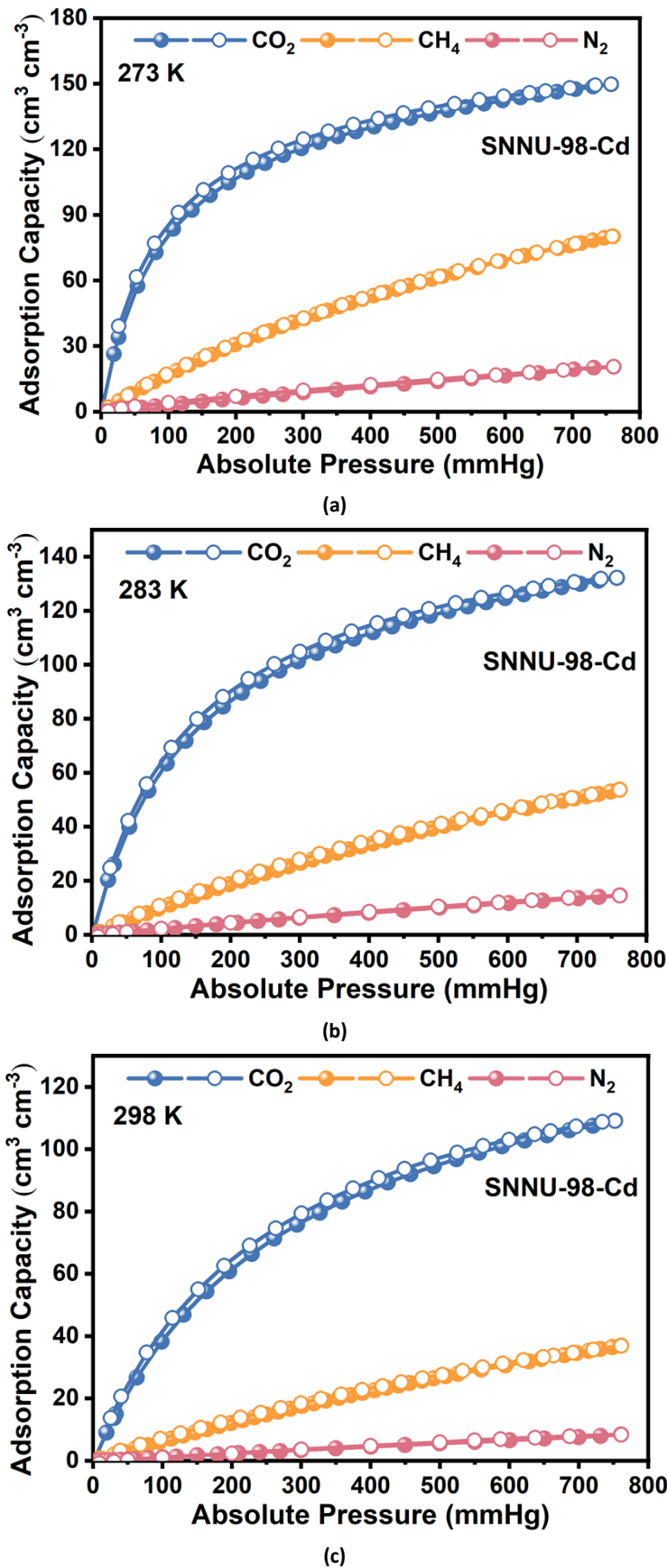


Figure S8. The CO_2 , CH_4 , and N_2 adsorption isotherms for SNNU-98-Cd at (a) 273, (b) 283, and (c) 298 K, respectively.

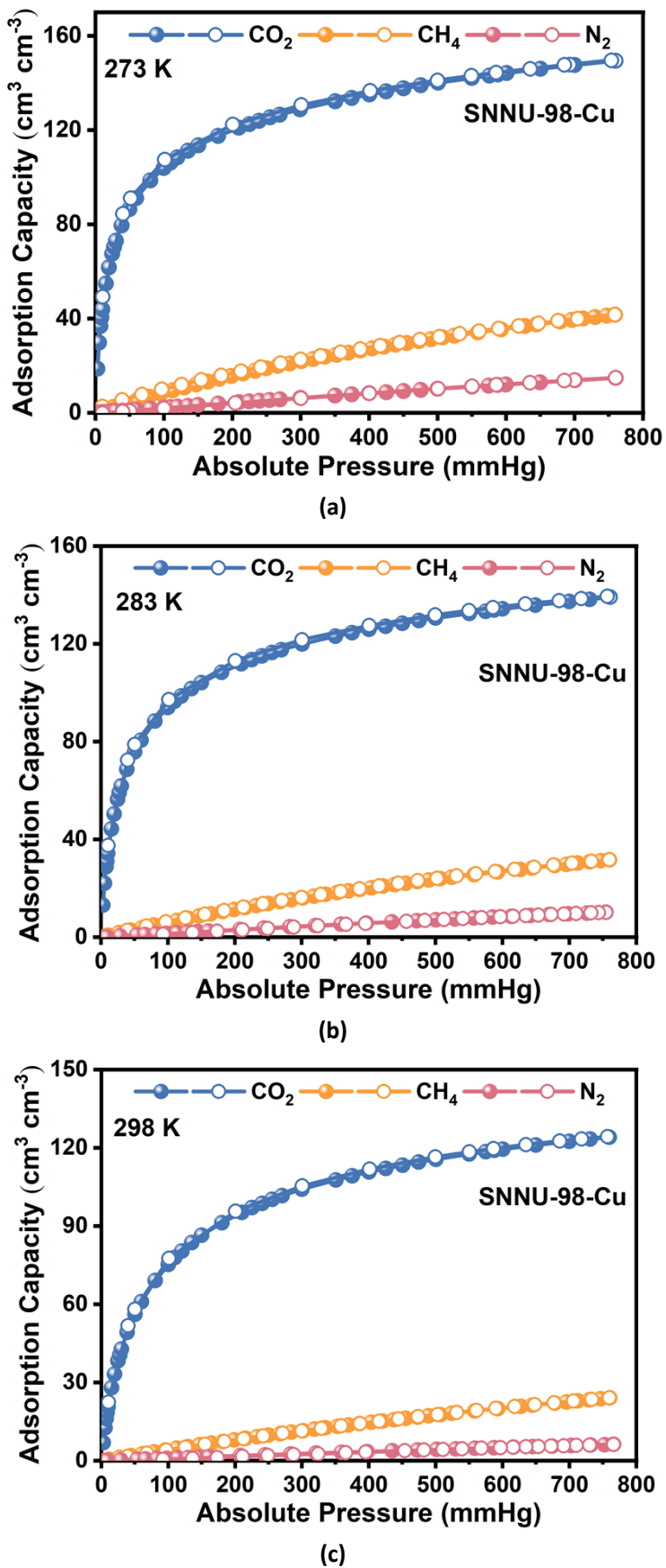
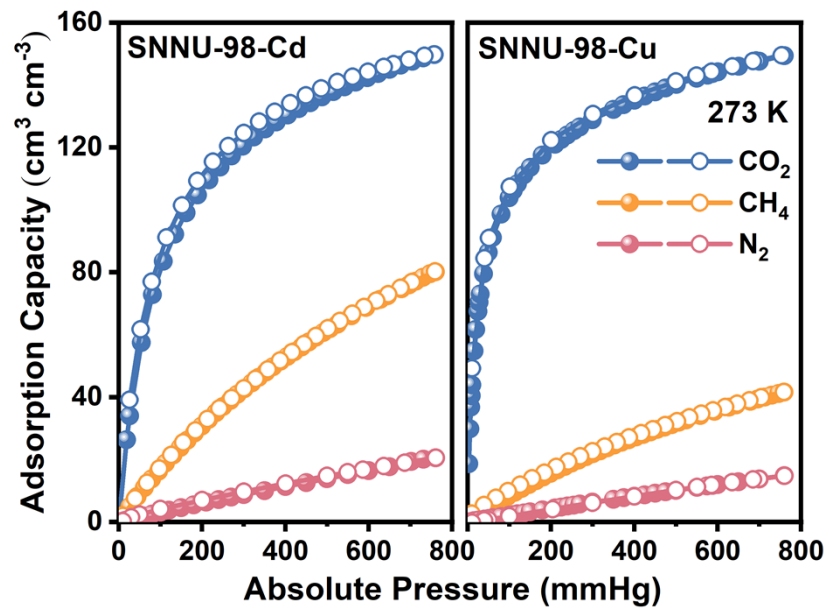
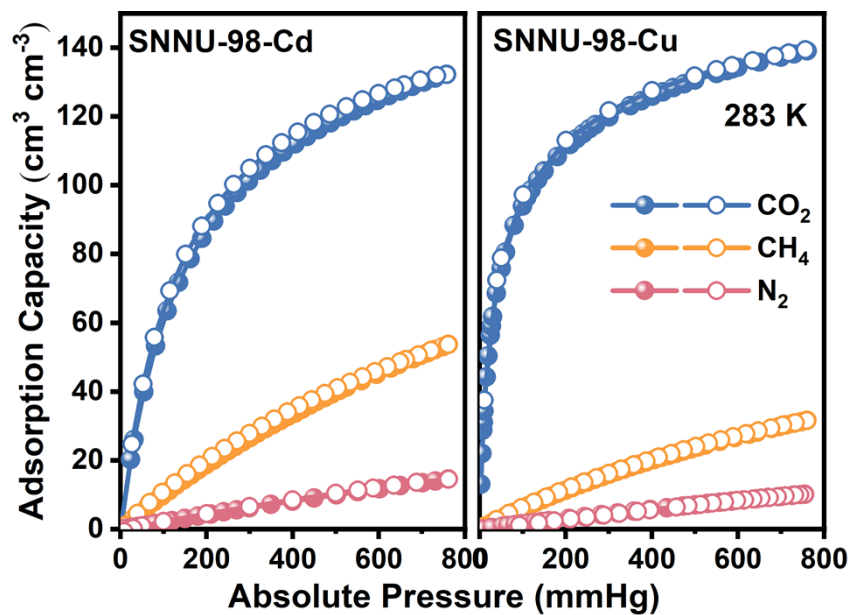


Figure S9. The CO_2 , CH_4 , and N_2 adsorption isotherms for SNNU-98-Cu at (a) 273, (b) 283, and (c) 298 K, respectively.



(a)



(b)

Figure S10. The adsorption isotherm comparison of SNNU-98-Cd/Cu at (a) 273, and (b) 283 K, respectively.

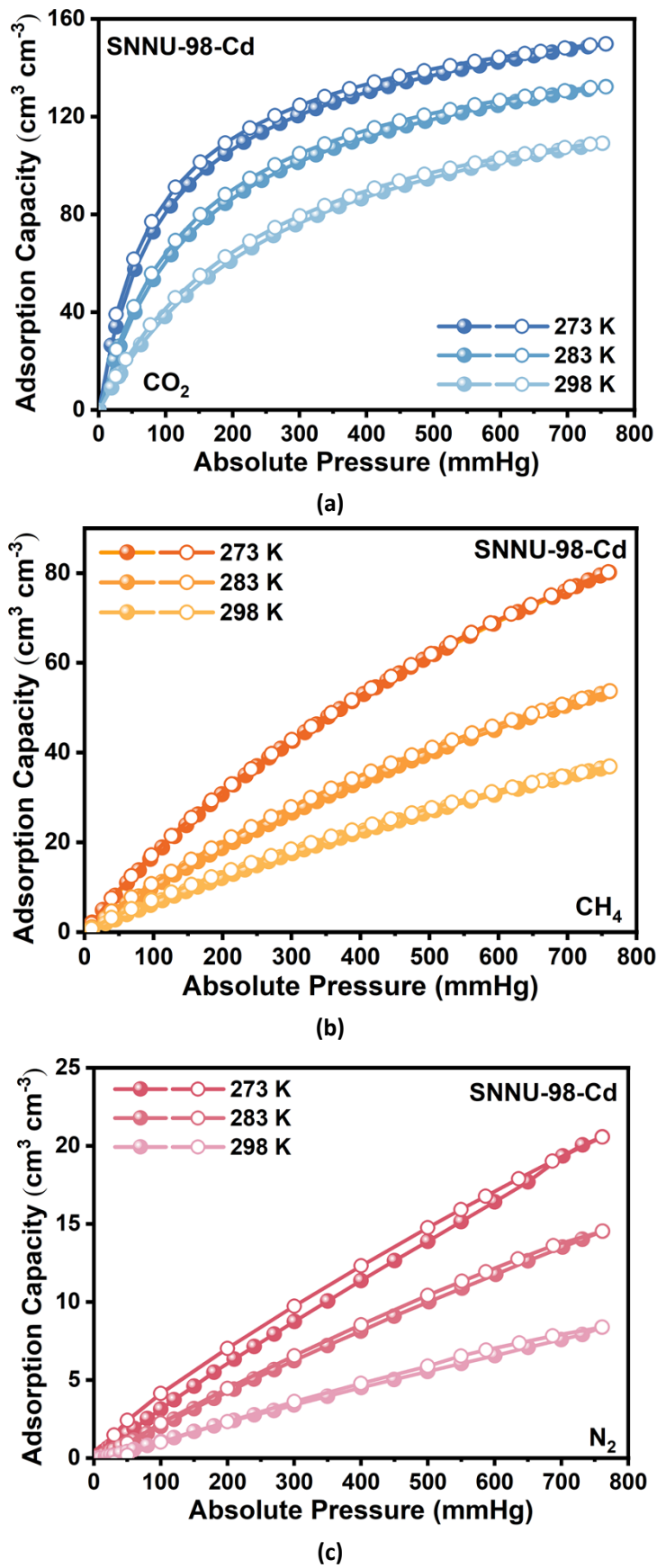
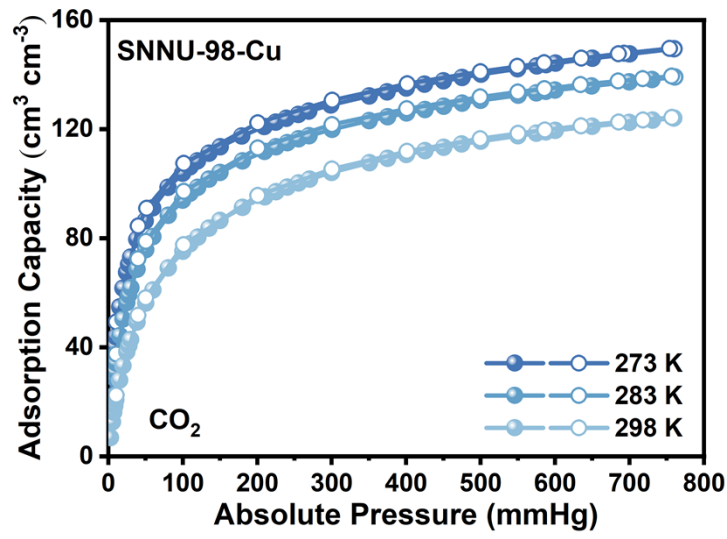
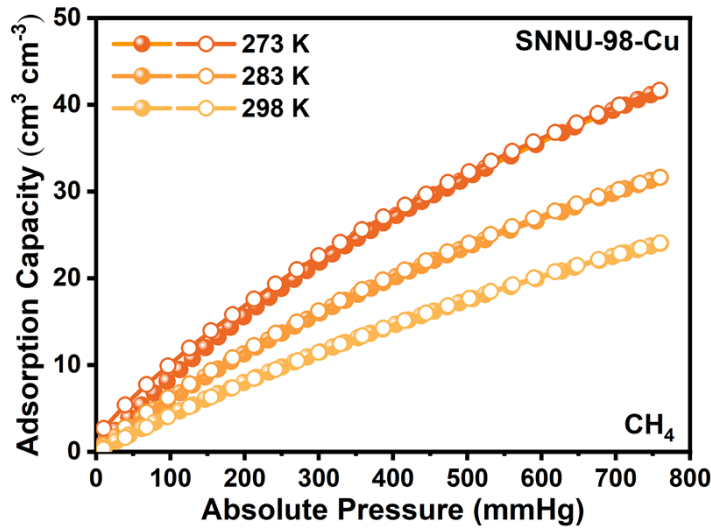


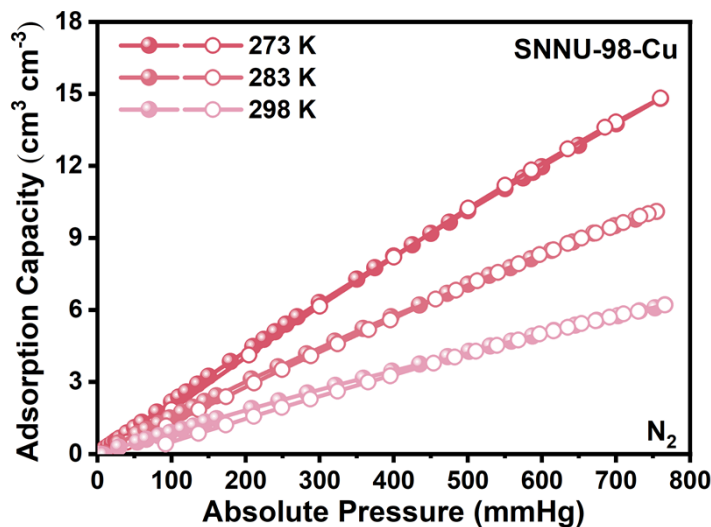
Figure S11. The (a) CO_2 , (b) CH_4 , and (c) N_2 adsorption isotherms for **SNNU-98-Cd** at 273, 283, and 298 K, respectively.



(a)



(b)



(c)

Figure S12. The (a) CO₂, (b) CH₄, and (c) N₂ adsorption isotherms for **SNNU-98-Cu** at 273, 283, and 298 K, respectively.

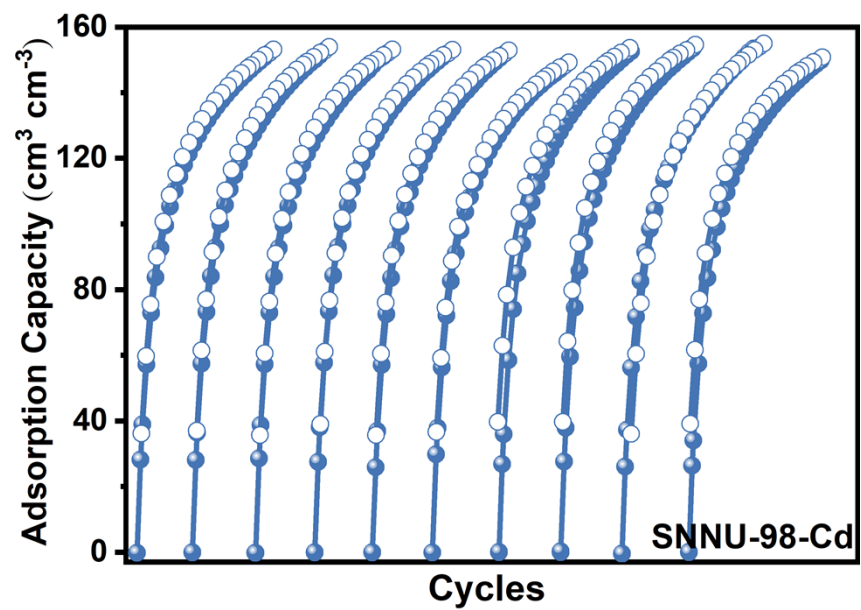


Figure S13. The cyclic stability of CO_2 adsorption of (a) SNNU-98-Cd at 273 K.

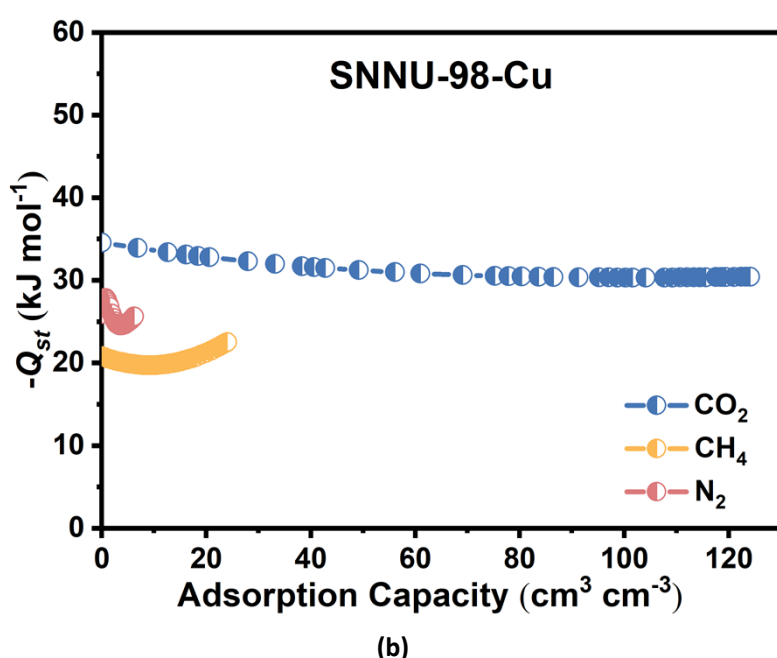
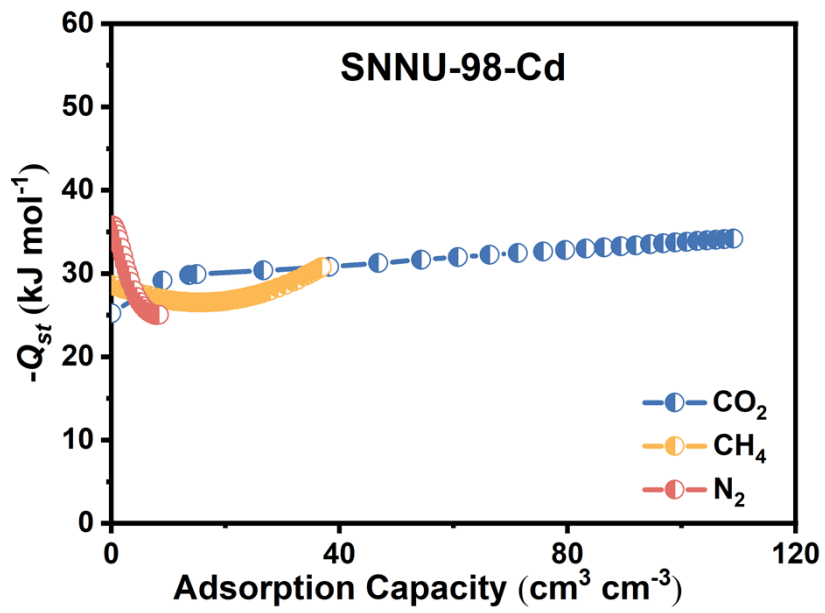


Figure S14. The adsorption enthalpy ($-Q_{st}$) of CO_2 , CH_4 , and N_2 for **SNNU-98-Cd** and **SNNU-98-Cu**.

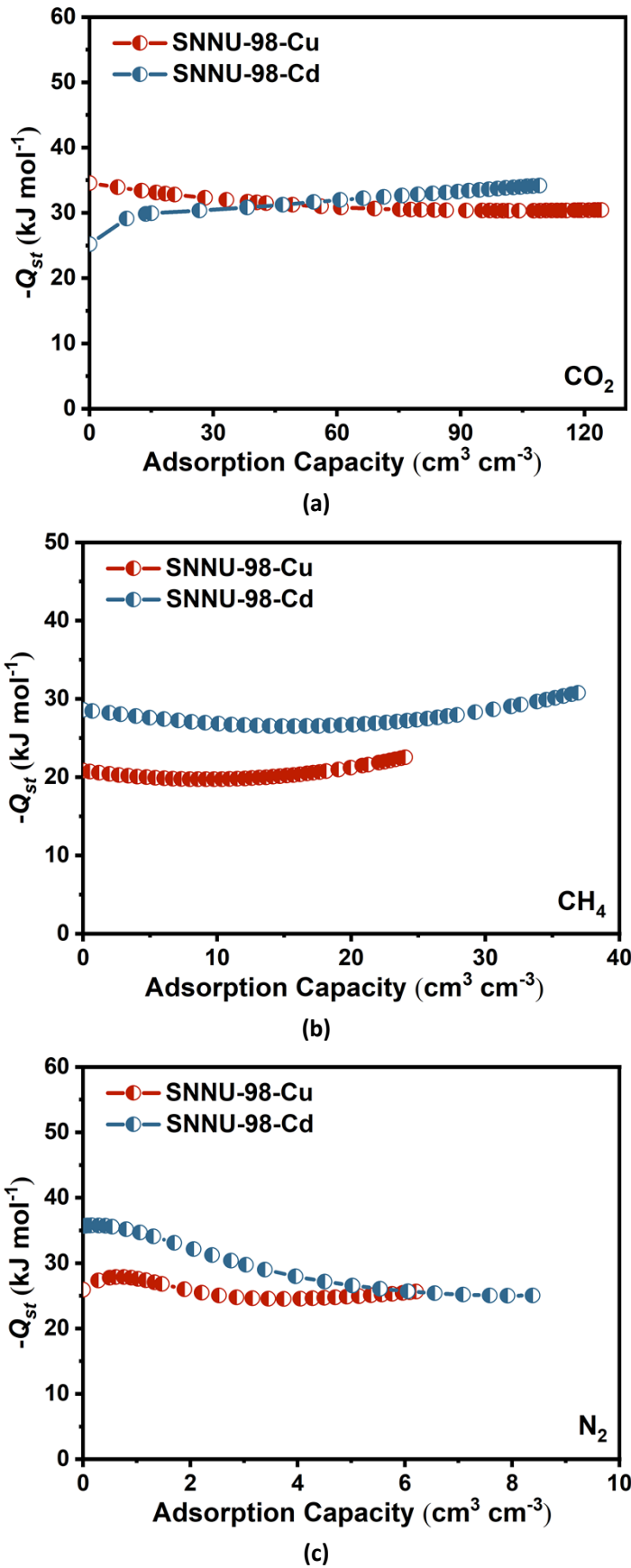


Figure S15. Comparison of the $-Q_{st}$ of (a) CO₂, (b) CH₄, and (c) N₂ between SNNU-98-Cu and SNNU-98-Cd.

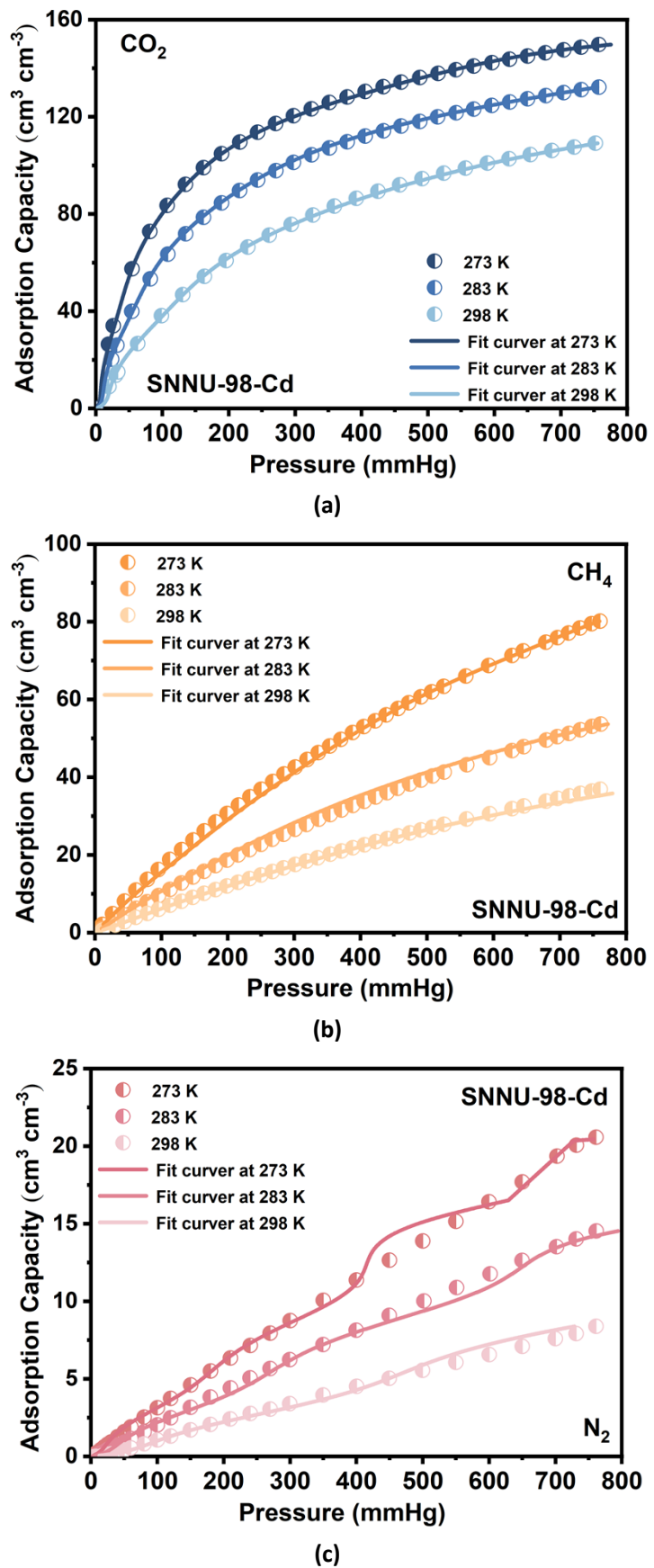
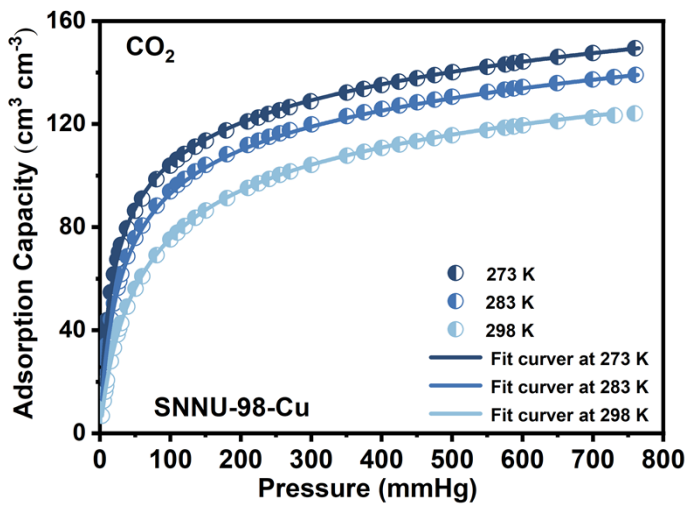
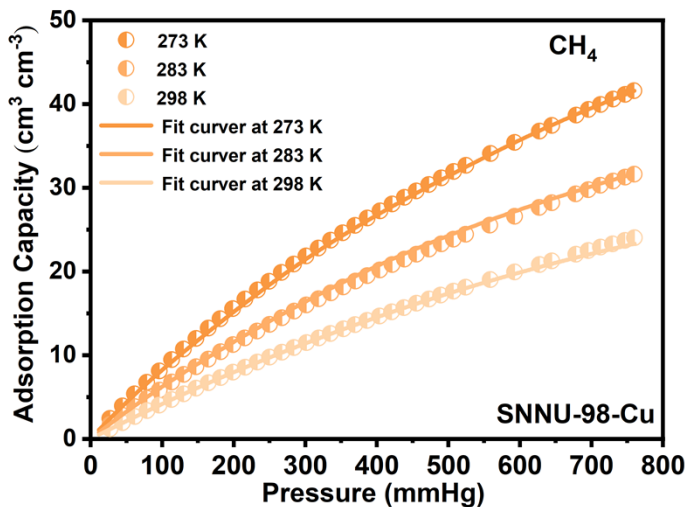


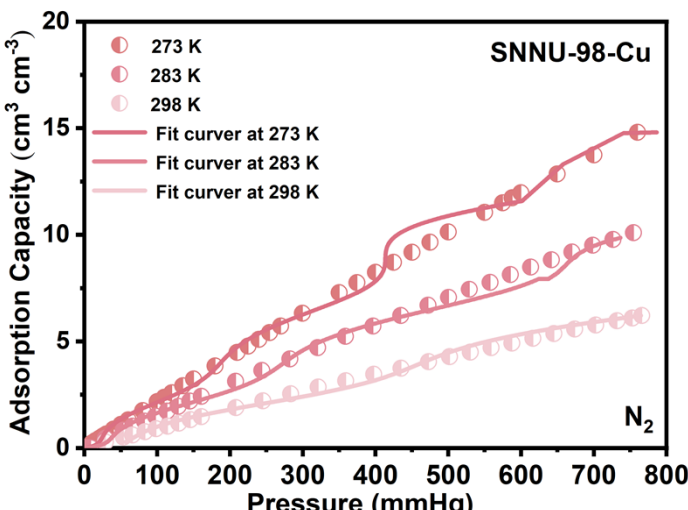
Figure S16. Fitted (a) CO_2 , (b) CH_4 , and (c) N_2 adsorption isotherms of **SNNU-98-Cd** measured at 273, 283, and 298 K.



(a)



(b)



(c)

Figure S17. Fitted (a) CO_2 , (b) CH_4 , and (c) N_2 adsorption isotherms of **SNNU-98-Cu** measured at 273, 283, and 298 K.

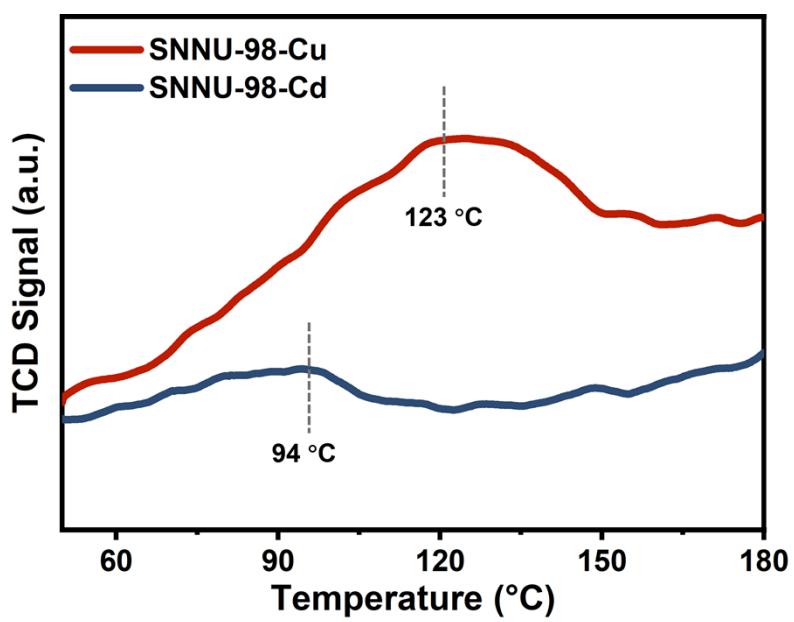
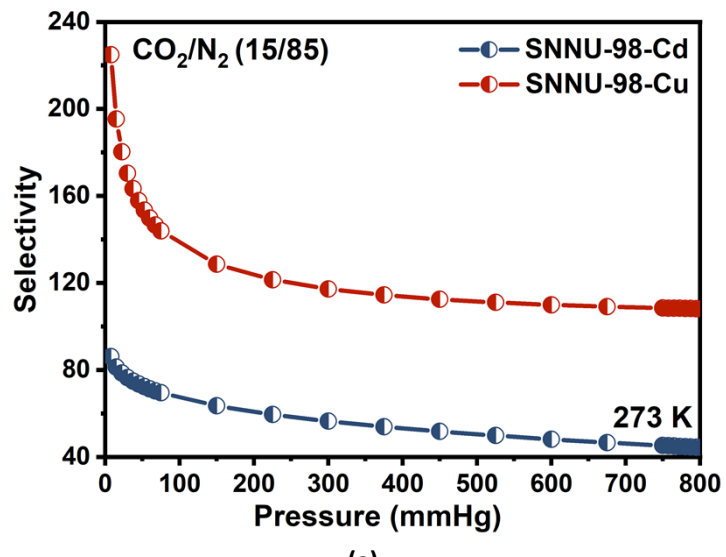
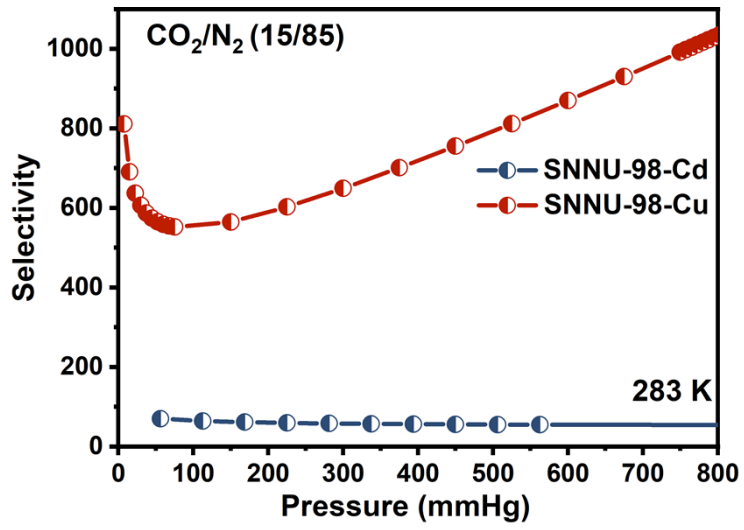


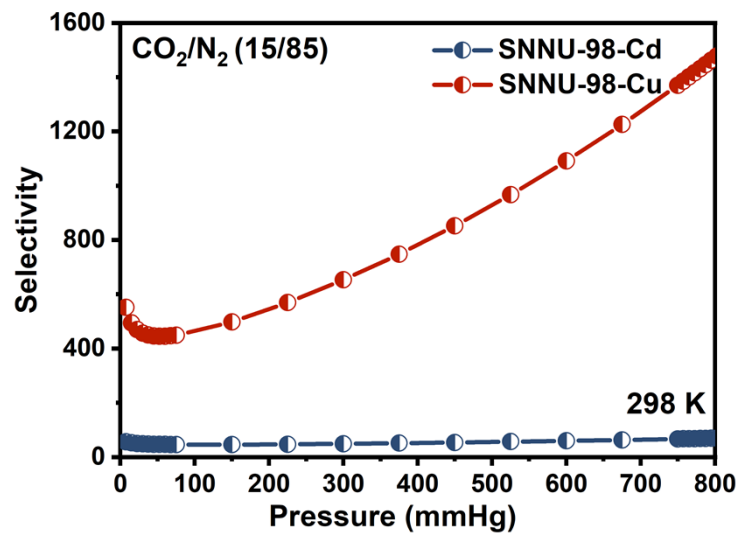
Figure S18. CO₂-TPD profiles of SNNU-98-Cd and SNNU-98-Cu.



(a)



(b)



(c)

Figure S19. Comparison of the CO_2/N_2 (15/85, v/v) IAST selectivity of SNNU-98-Cd and SNNU-98-Cu at (a) 273, (b) 283, and (c) 298 K, respectively.

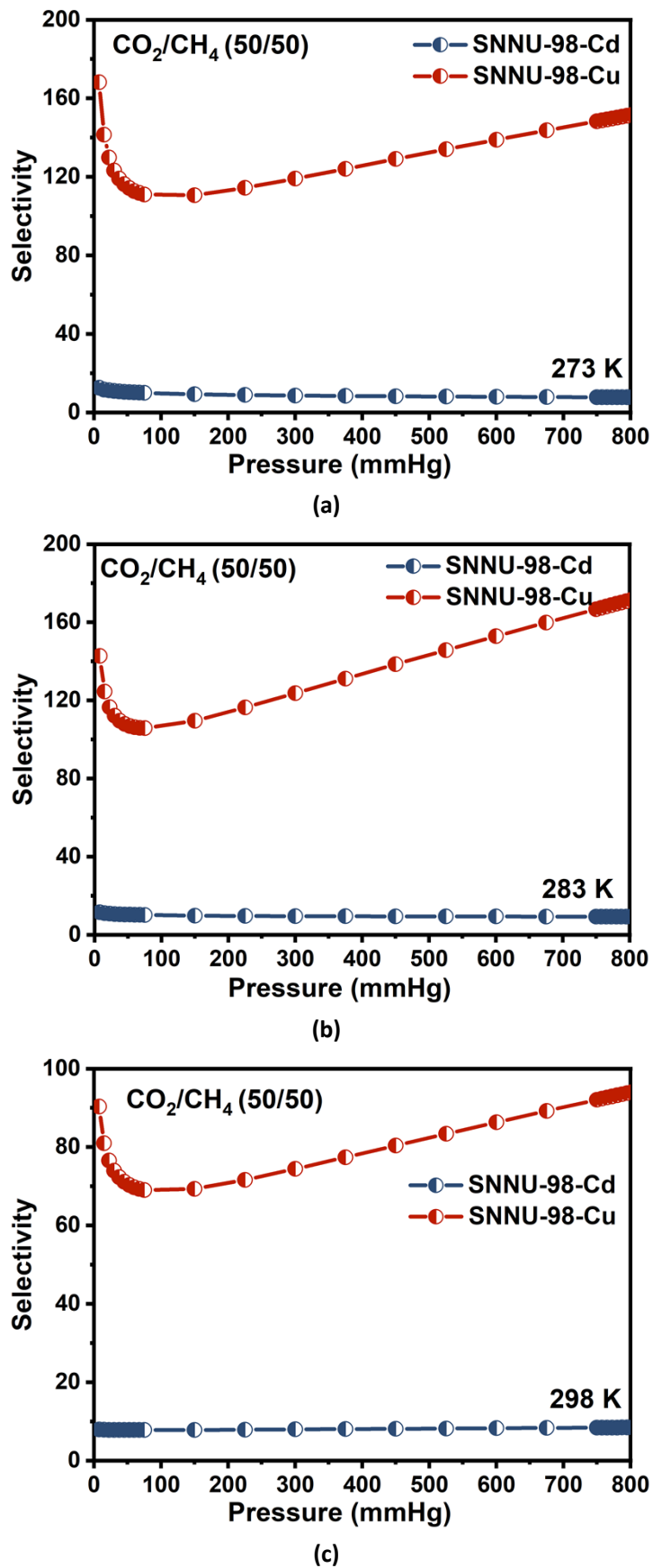


Figure S20. Comparison of the CO_2/CH_4 (50/50, v/v) IAST selectivity of **SNNU-98-Cd** and **SNNU-98-Cu** at (a) 273, (b) 283, and (c) 298 K, respectively.

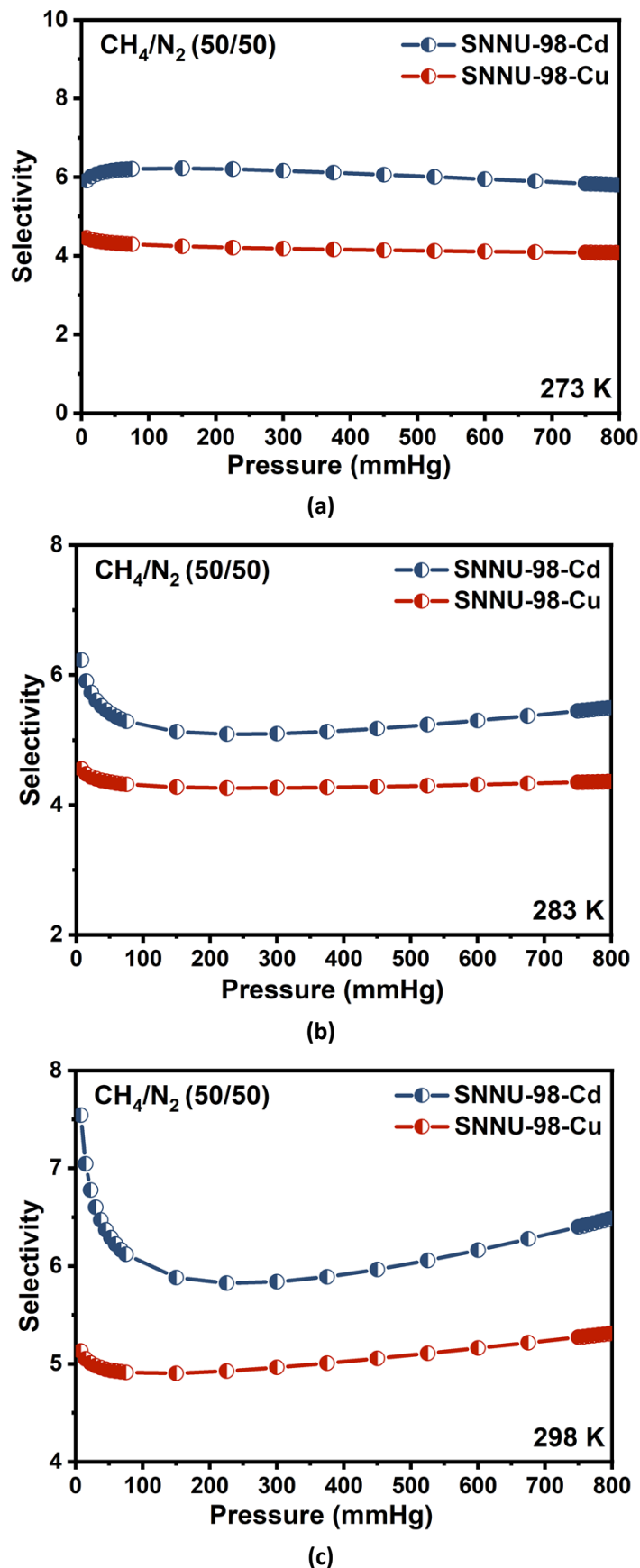


Figure S21. Comparison of the CH₄/N₂ (50/50, v/v) IAST selectivity of SNNU-98-Cd and SNNU-98-Cu at (a) 273, (b) 283, and (c) 298 K, respectively.

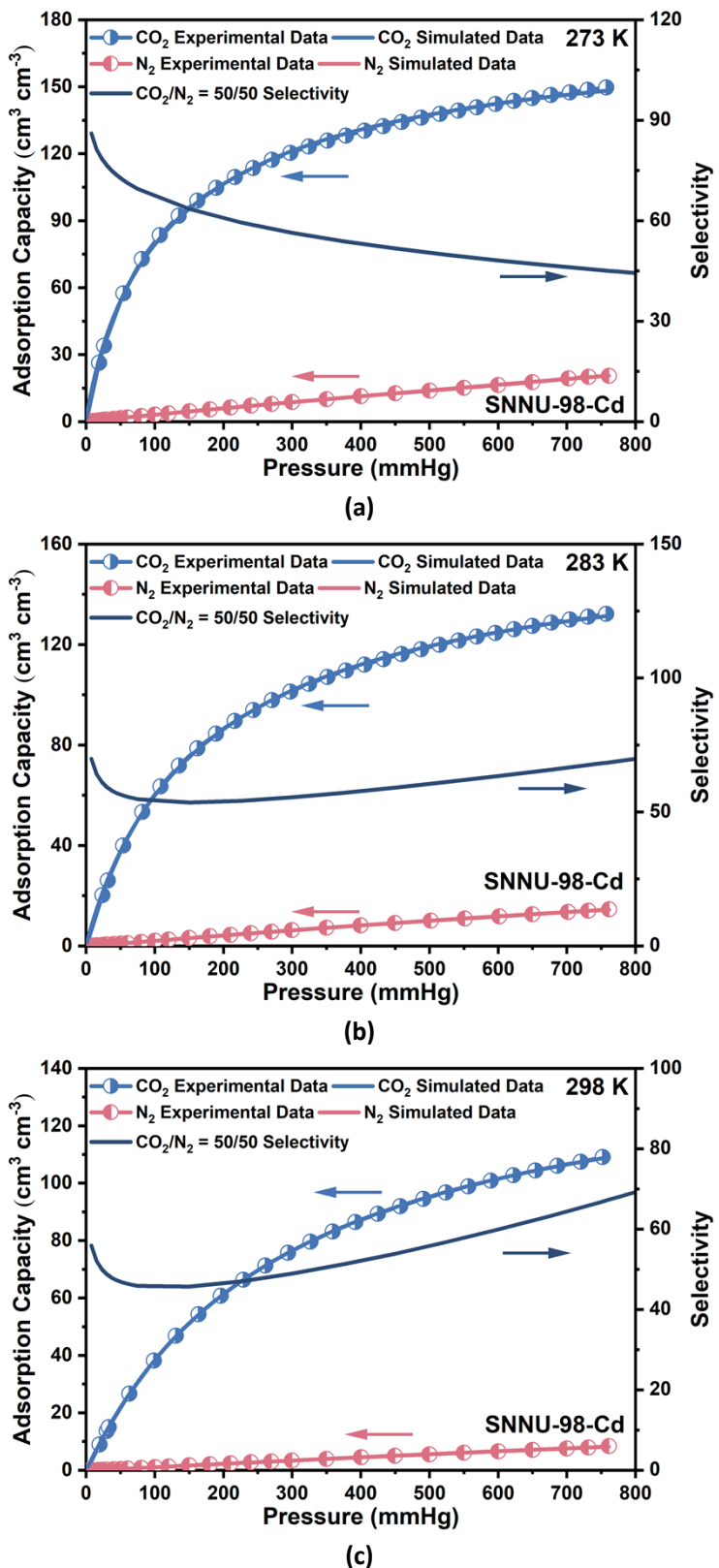


Figure S22. Comparison of experimental isotherms and simulated isotherms (Left Y axis), and mixture adsorption selectivity predicted by IAST (Right Y axis) of SNNU-98-Cd for CO_2/N_2 (15/85) at (a) 273, (b) 283, and (c) 298 K.

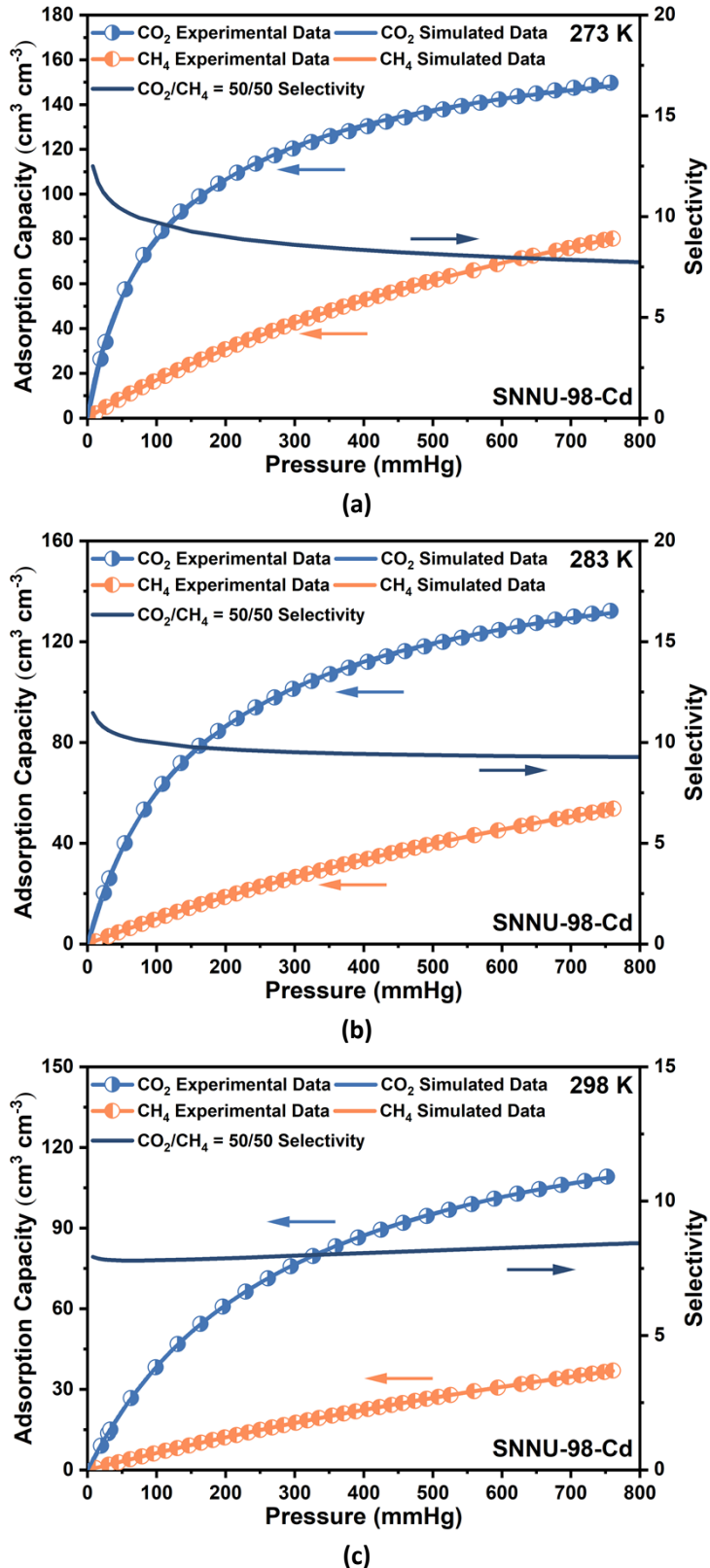


Figure S23. Comparison of experimental isotherms and simulated isotherms (Left Y axis), and mixture adsorption selectivity predicted by IAST (Right Y axis) of **SNNU-98-Cd** for equimolar binary-mixture CO_2/CH_4 at (a) 273, (b) 283, and (c) 298 K.

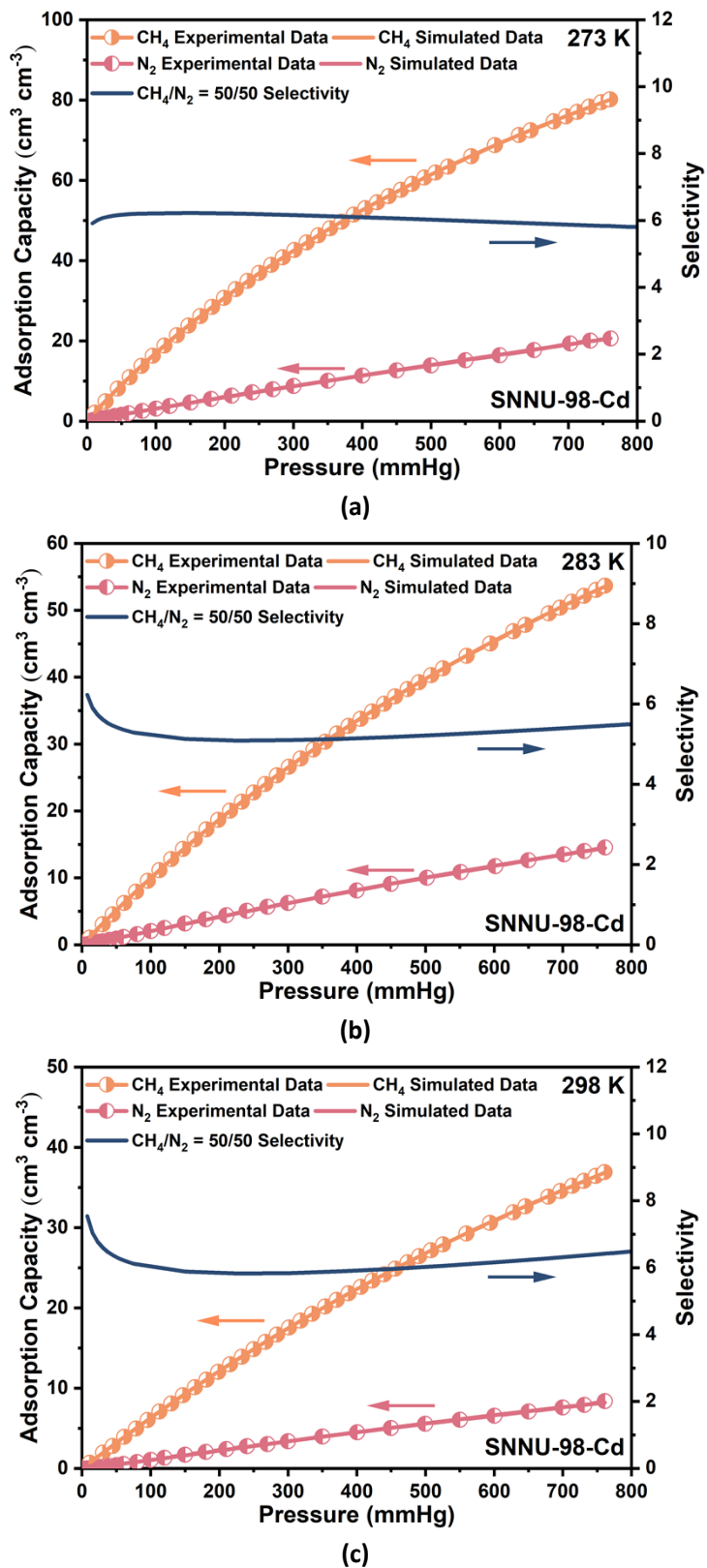


Figure S24. Comparison of experimental isotherms and simulated isotherms (Left Y axis), and mixture adsorption selectivity predicted by IAST (Right Y axis) of SNNU-98-Cd for equimolar binary-mixture CH_4/N_2 at (a) 273, (b) 283, and (c) 298 K.

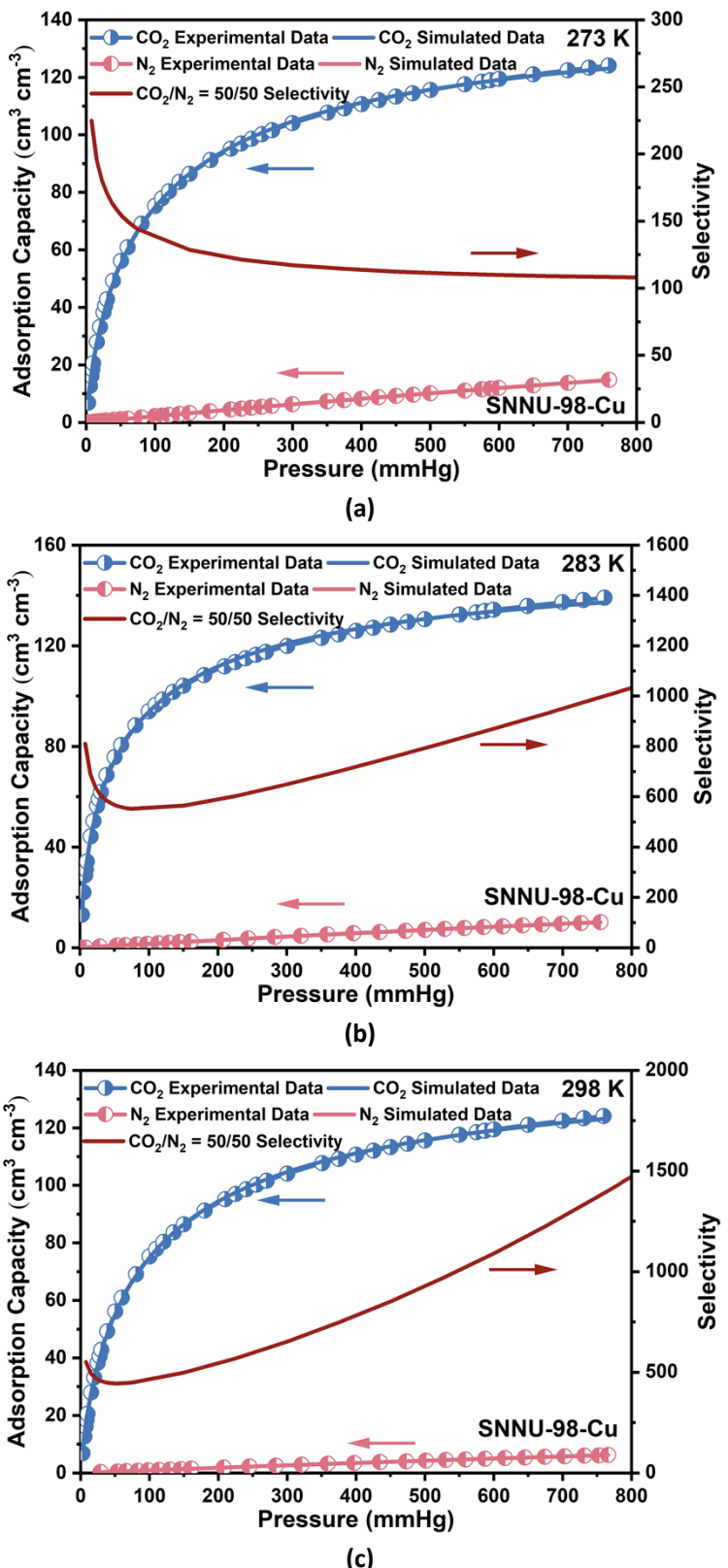


Figure S25. Comparison of experimental isotherms and simulated isotherms (Left Y axis), and mixture adsorption selectivity predicted by IAST (Right Y axis) of SNNU-98-Cu for CO_2/N_2 (15/85) at (a) 273, (b) 283, and (c) 298 K.

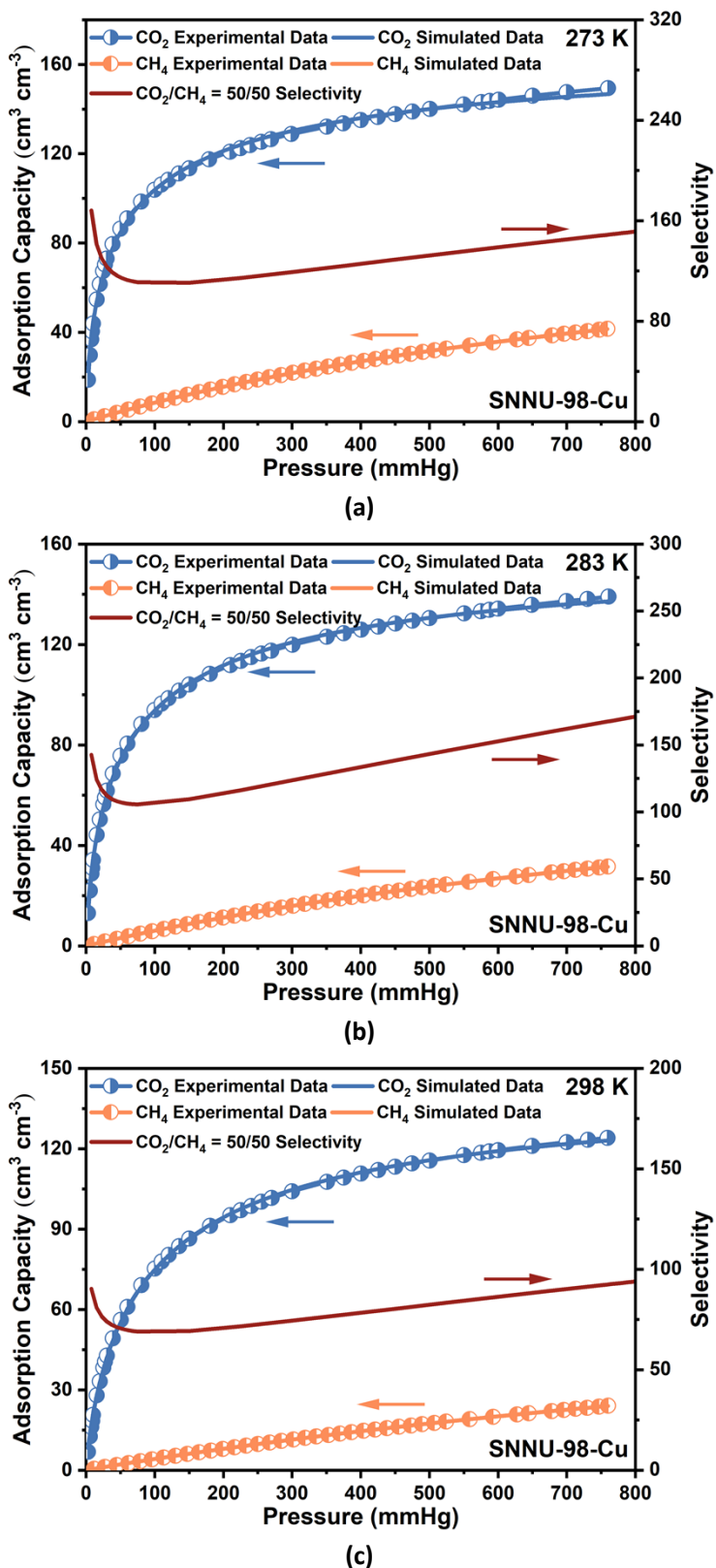


Figure S26. Comparison of experimental isotherms and simulated isotherms (Left Y axis), and mixture adsorption selectivity predicted by IAST (Right Y axis) of **SNNU-98-Cu** for equimolar binary-mixture CO₂/CH₄ at (a) 273, (b) 283, and (c) 298 K.

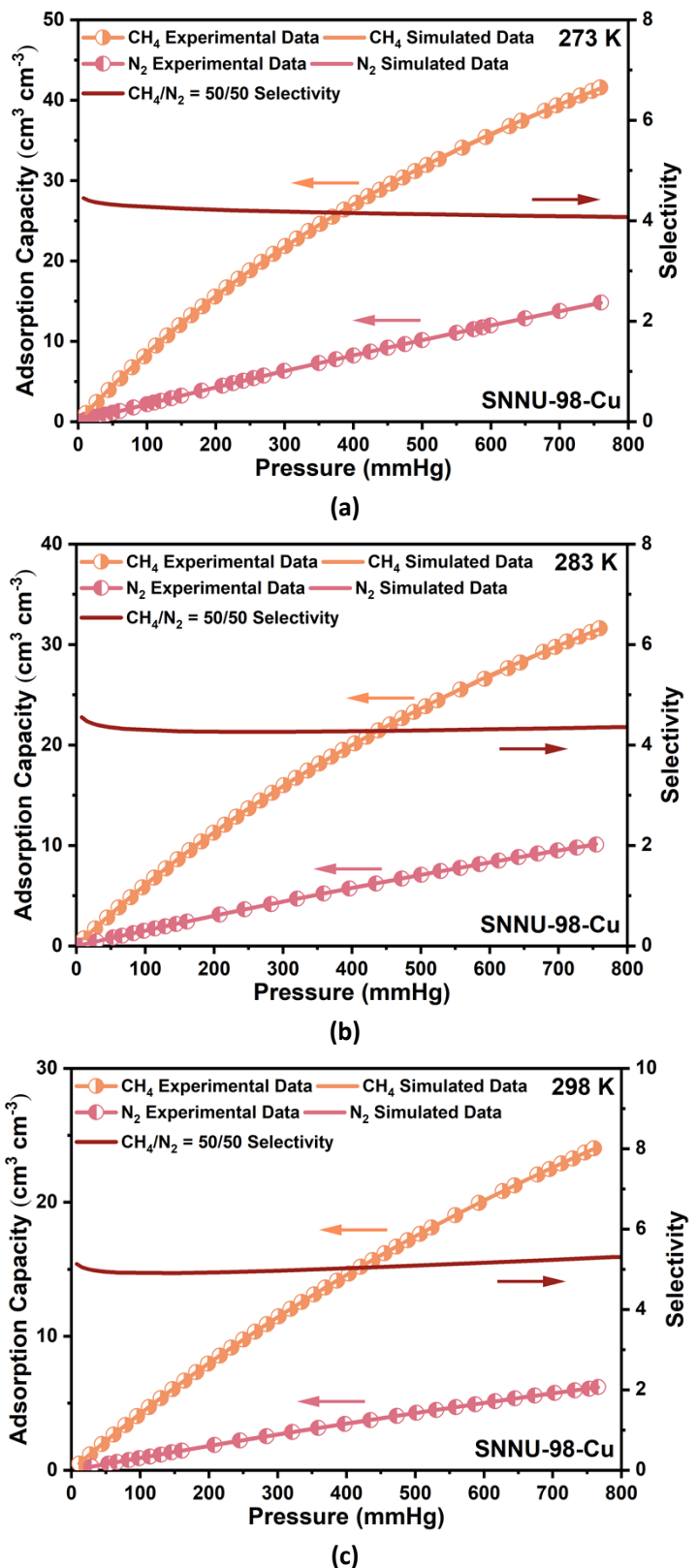


Figure S27. Comparison of experimental isotherms and simulated isotherms (Left Y axis), and mixture adsorption selectivity predicted by IAST (Right Y axis) of SNNU-98-Cu for equimolar binary-mixture CH_4/N_2 at (a) 273, (b) 283, and (c) 298 K.

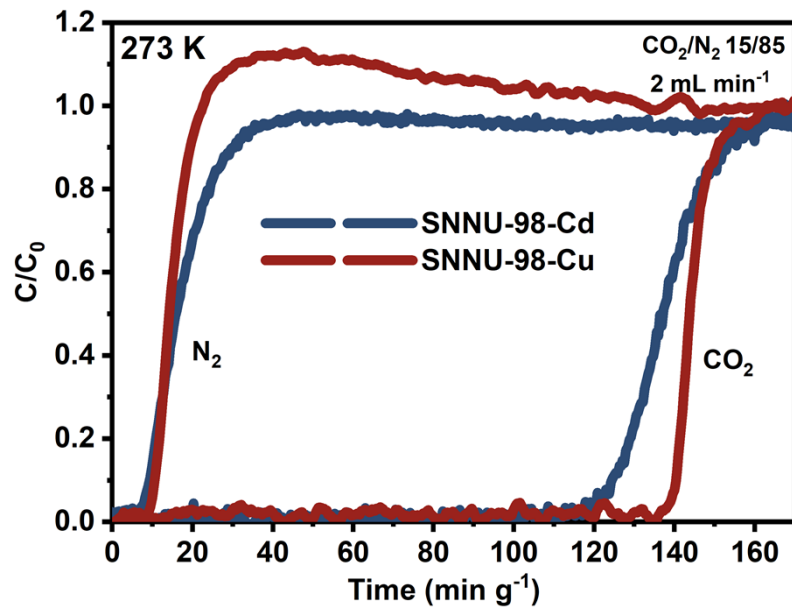


Figure S28. The experimental breakthrough curves for CO_2/N_2 (15/85, v/v) gas mixtures of **SNNU-98-Cd/Cu** with a flow rate of 2 ml min^{-1} at 273 K and 1 bar.

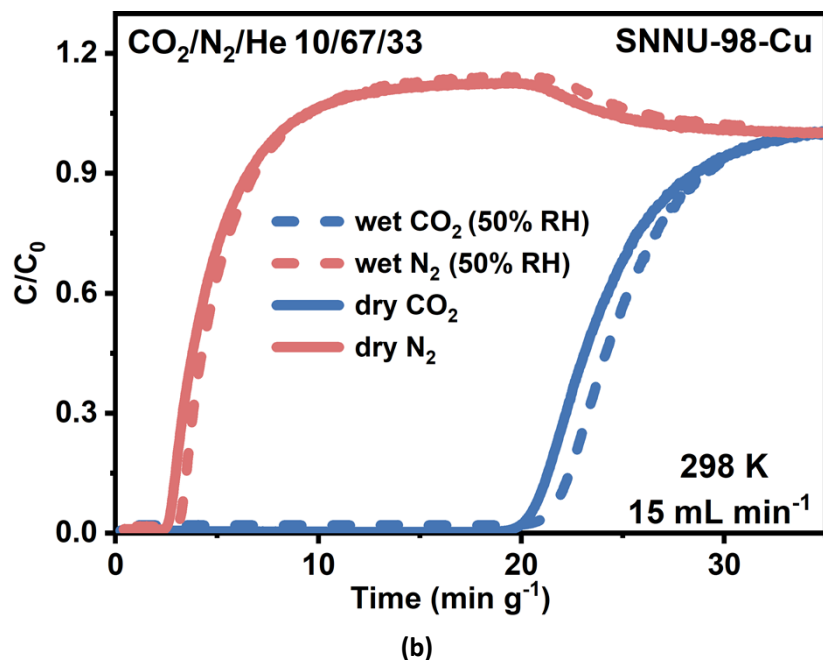
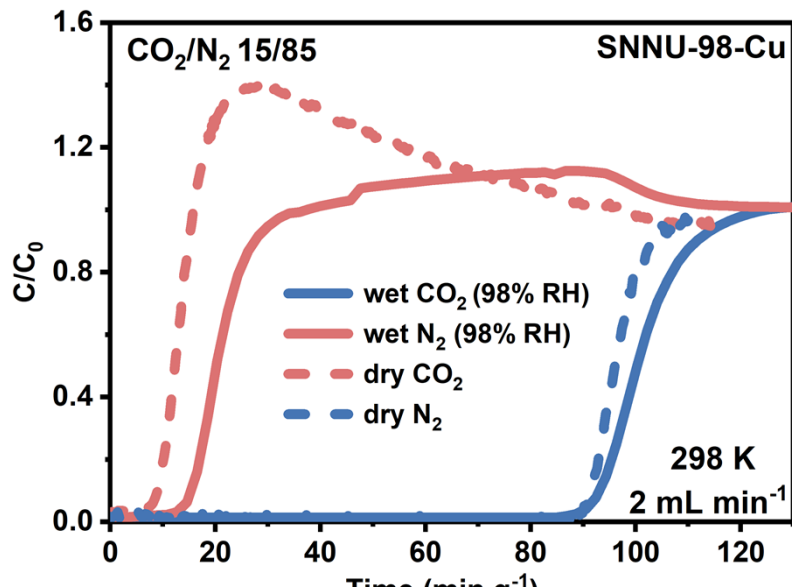


Figure S29. The experimental breakthrough curves of the CO₂/N₂ gas mixtures under different test conditions in the moist and dry environments of SNNU-98-Cu.

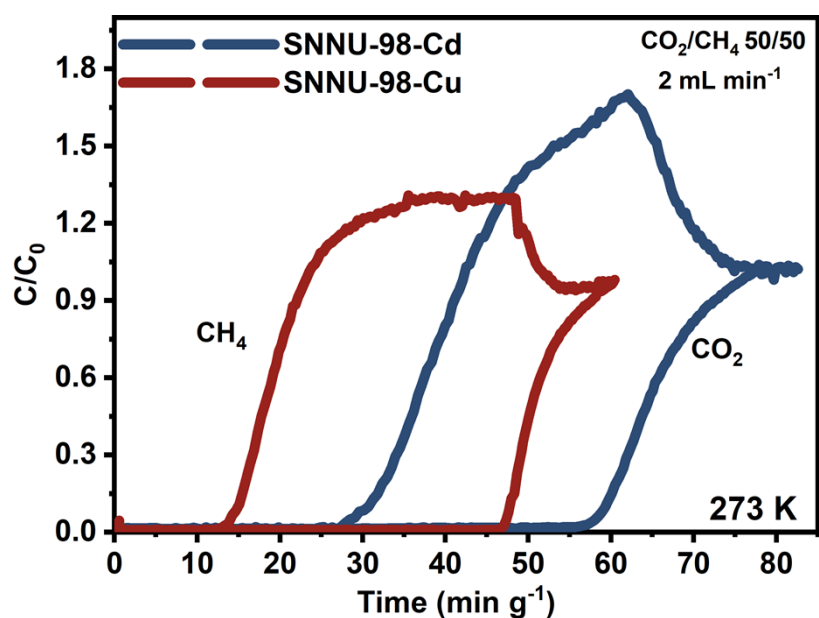
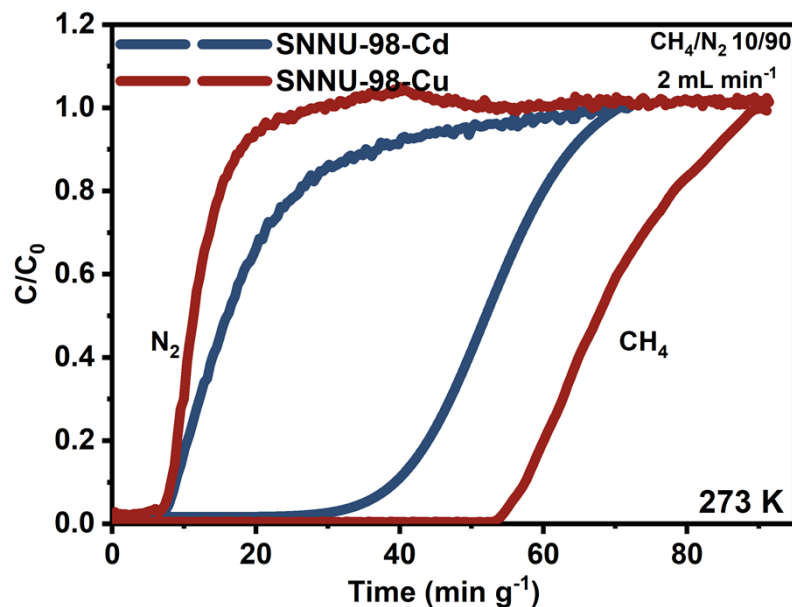
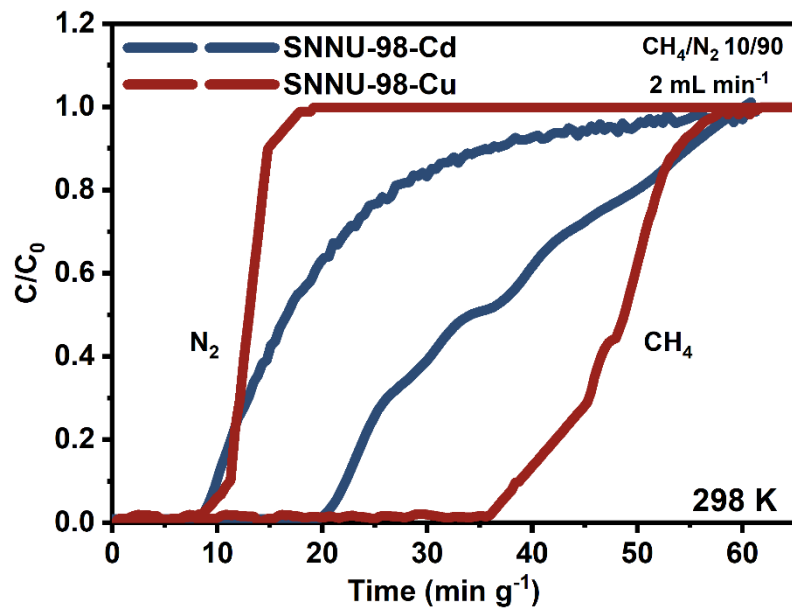


Figure S30. The experimental breakthrough curves for CO_2/CH_4 (50/50, v/v) gas mixtures of SNNU-98-Cd/Cu with a flow rate of 2 ml min^{-1} at 273 K and 1 bar.



(a)



(b)

Figure S31. The experimental breakthrough curves for CH_4/N_2 (10/90, v/v) gas mixtures of **SNNU-98-Cd/Cu** with a flow rate of 2 ml min⁻¹ at (a) 273 and (b) 298 K and 1 bar.

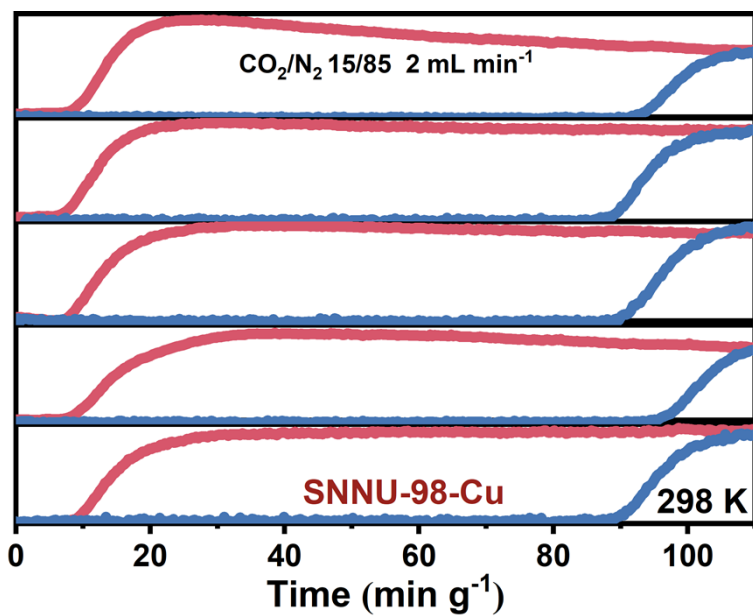


Figure S32. Cycling dynamic breakthrough tests for CO_2/N_2 (15/85, v/v) gas mixtures on **SNNU-98-Cu** with a flow rate of 2 ml min^{-1} at 298 K and 1 bar.

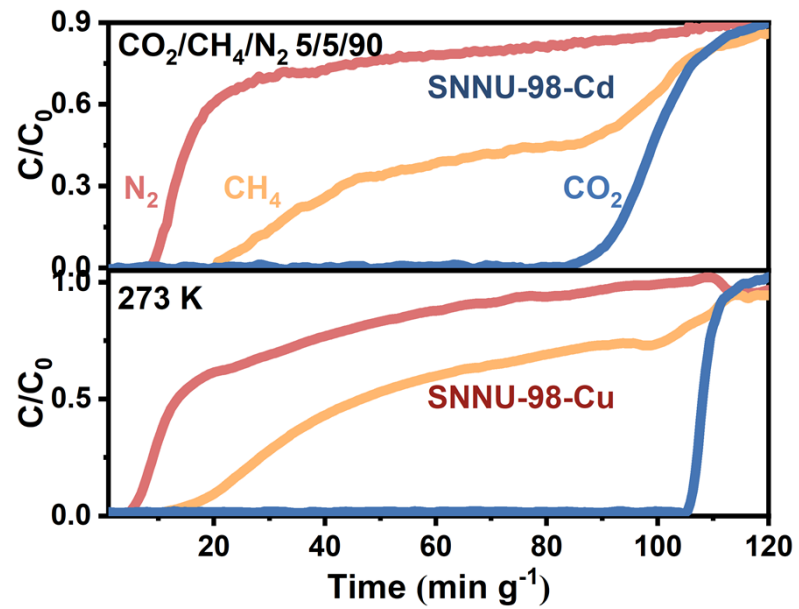
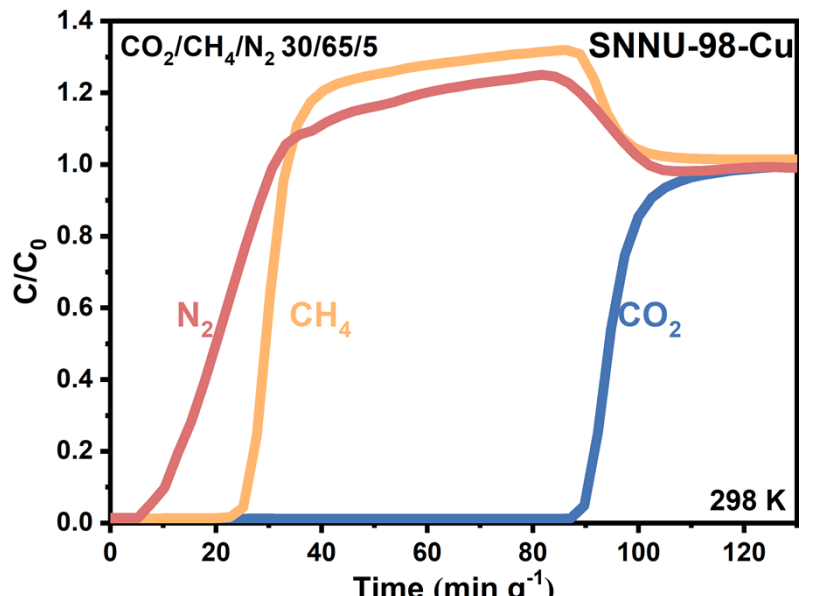
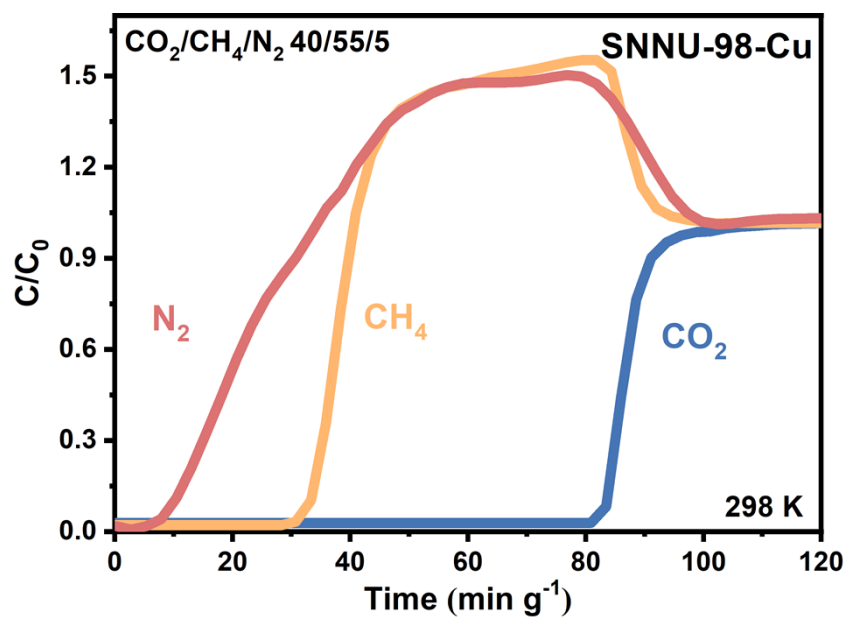


Figure S33. The experimental breakthrough curves for $\text{CO}_2/\text{CH}_4/\text{N}_2$ (5/5/90, v/v/v) gas mixtures of **SNNU-98-Cd/Cu** at 273 K and 1 bar.



(a)



(b)

Figure S34. The experimental breakthrough curves for (a) $\text{CO}_2/\text{CH}_4/\text{N}_2$ (30/65/5, v/v/v) and (b) $\text{CO}_2/\text{CH}_4/\text{N}_2$ (40/55/5, v/v/v) gas mixtures of SNNU-98-Cu at 298 K and 1 bar.

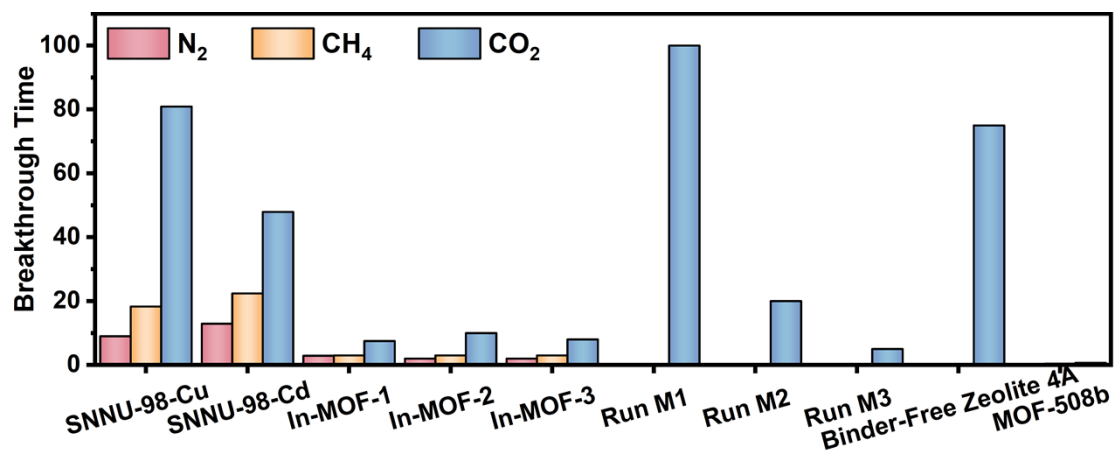


Figure S35. Comparison of CO₂/CH₄/N₂ three-component separation properties of currently studied MOF materials.

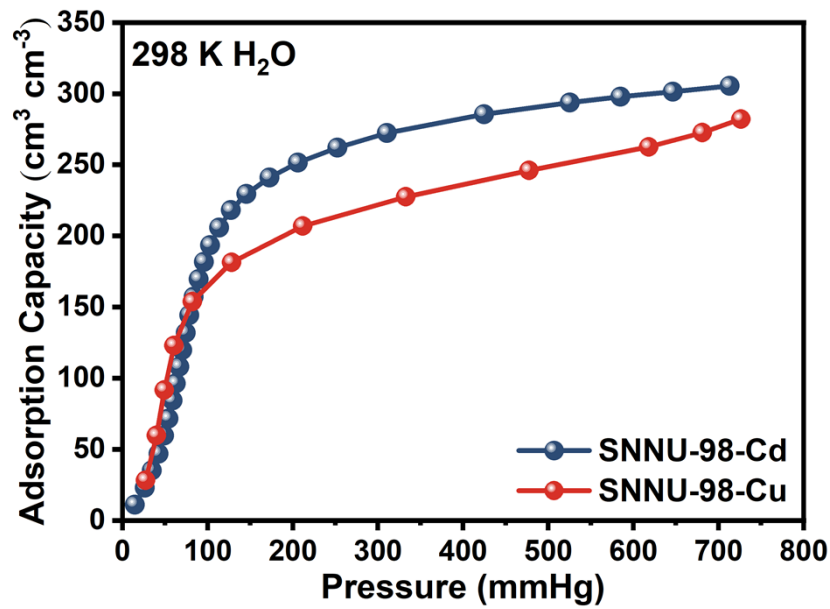


Figure S36. Water vapor adsorption of SNNU-98-Cd/Cu at 298 K and 1 bar.

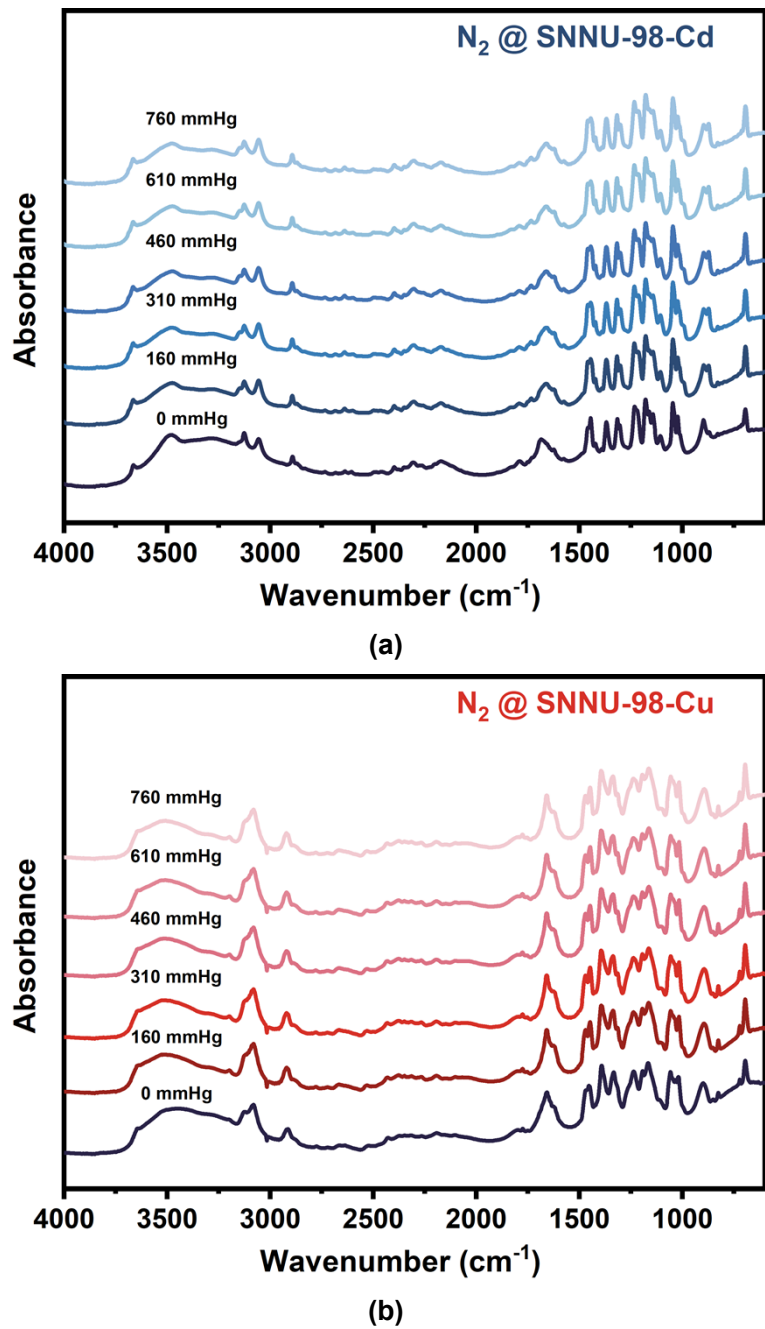


Figure S37. In situ IR spectra for N₂ in SNNU-98-Cd/Cu.

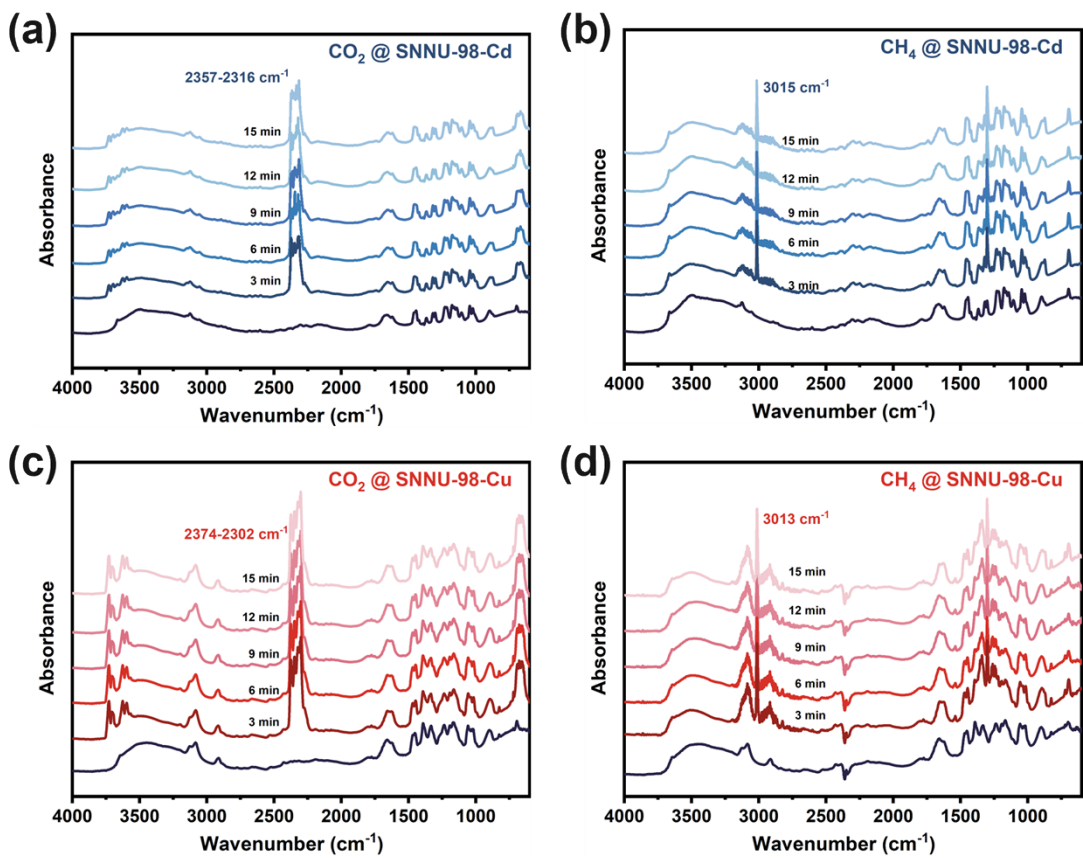


Figure S38. In situ IR spectra for CO_2 and CH_4 in SNNU-98-Cd/Cu at different time and 1 bar.

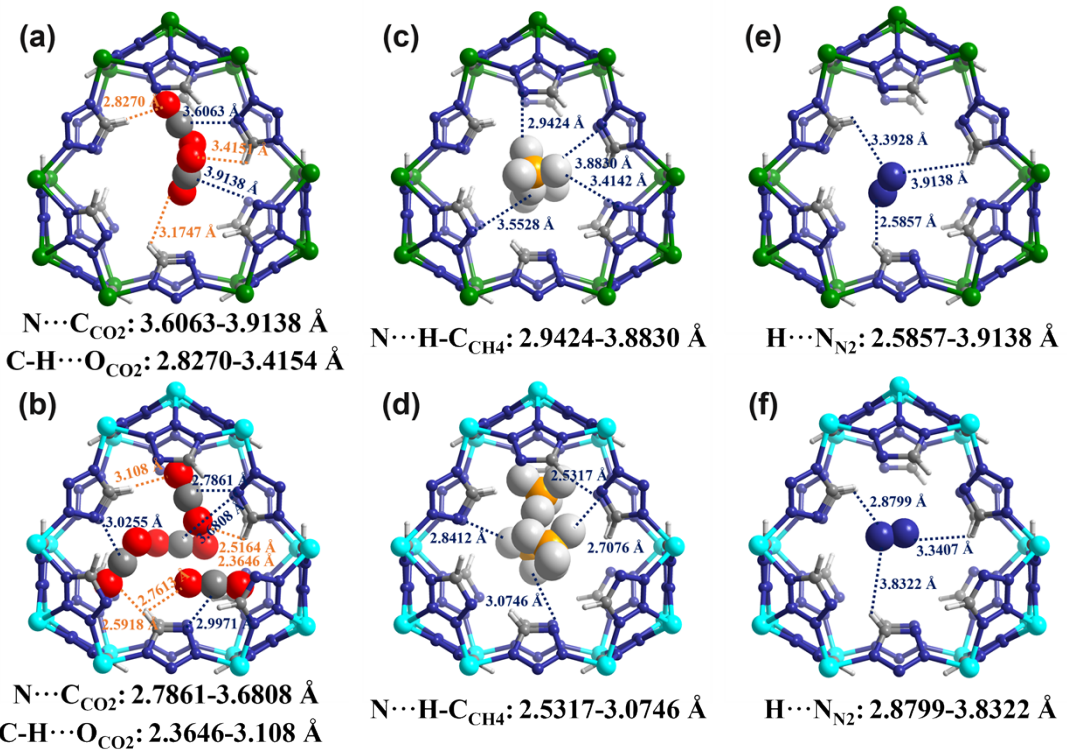


Figure S39. GCMC simulated adsorption binding sites in **SNNU-98-Cd** for a) CO_2 , c) CH_4 , and e) N_2 ; GCMC simulated adsorption binding sites in **SNNU-98-Cu** for b) CO_2 , d) CH_4 , and f) N_2 .

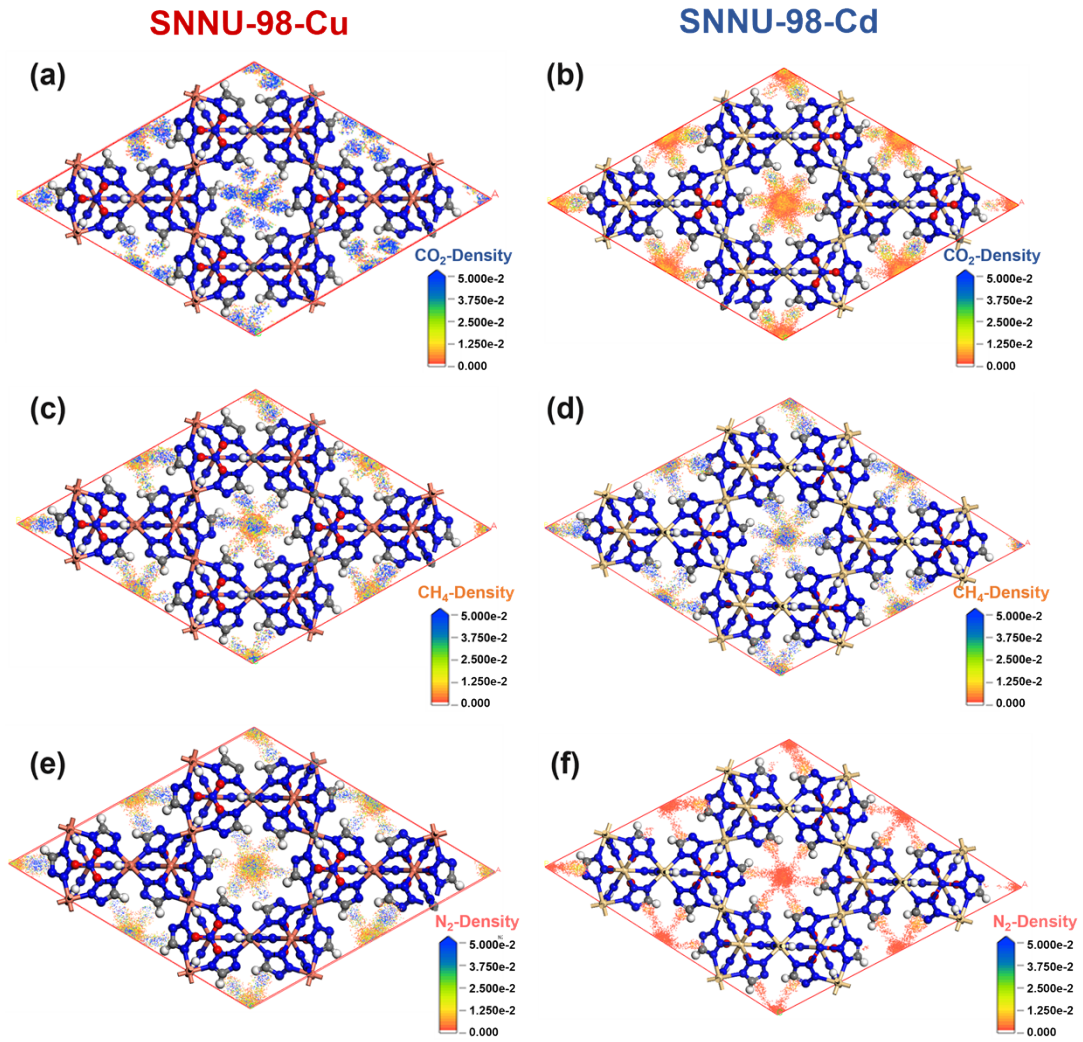


Figure S40. GCMC simulated density distributions in **SNNU-98-Cd/Cu** at 298 K and 1 bar of CO₂, CH₄, and N₂.

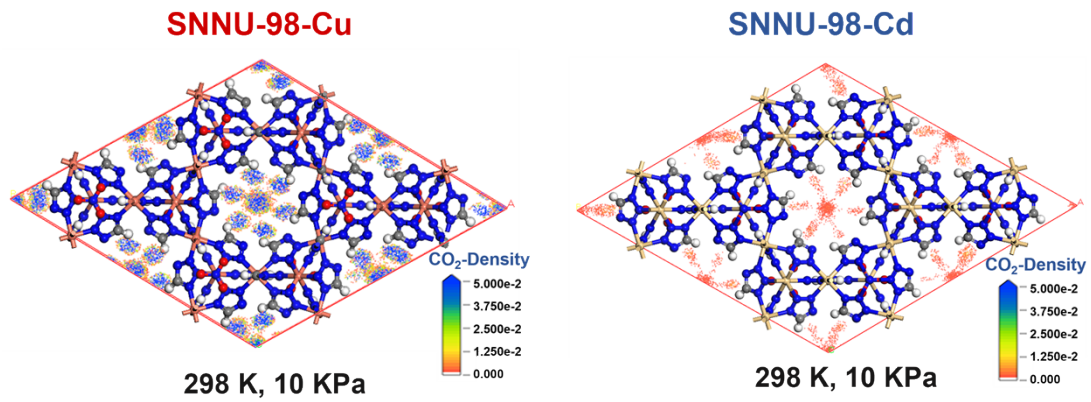


Figure S41. GCMC simulated density distributions in **SNNU-98-Cd/Cu** at 298 K and 0.1 bar of CO₂.

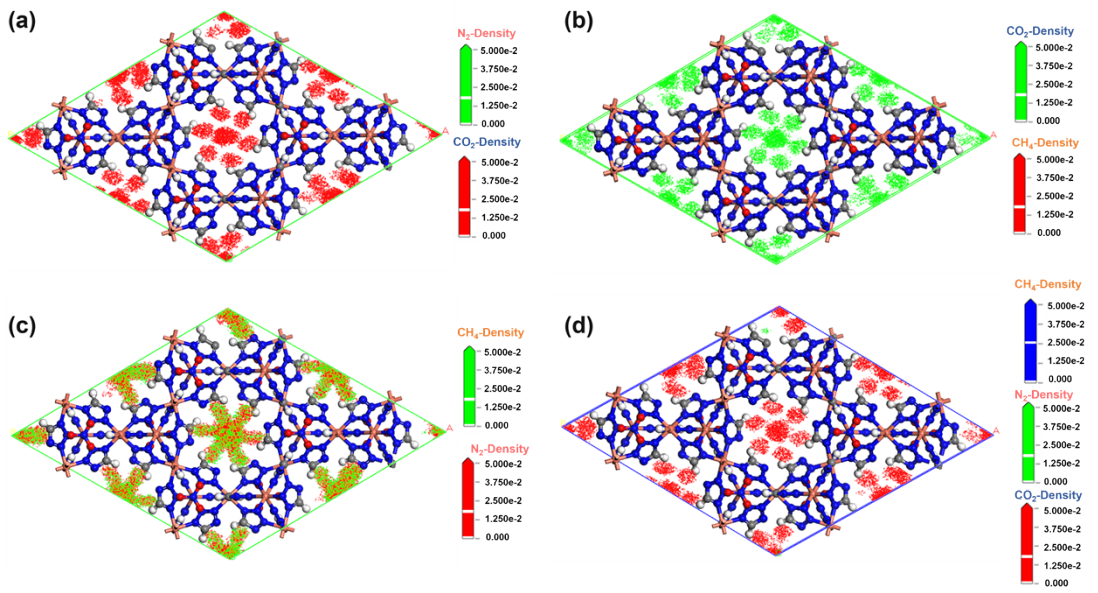


Figure S42. GCMC simulated density distributions in **SNNU-98-Cu** at 298 K and 1 bar of (a) CO₂/N₂, (b) CO₂/CH₄, (c) CH₄/N₂, and (d) CO₂/CH₄/N₂.

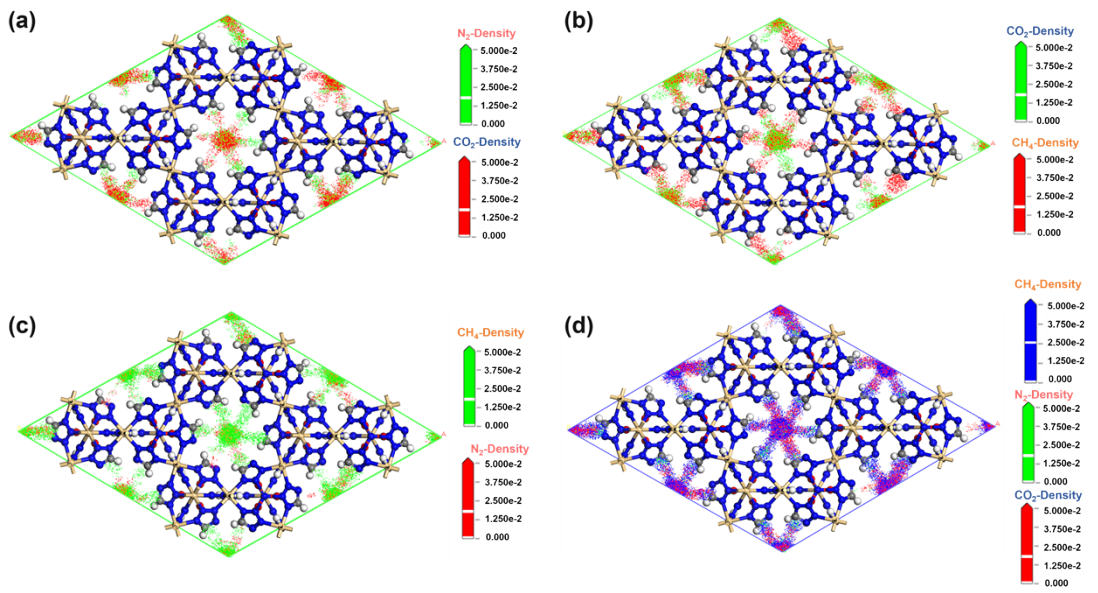
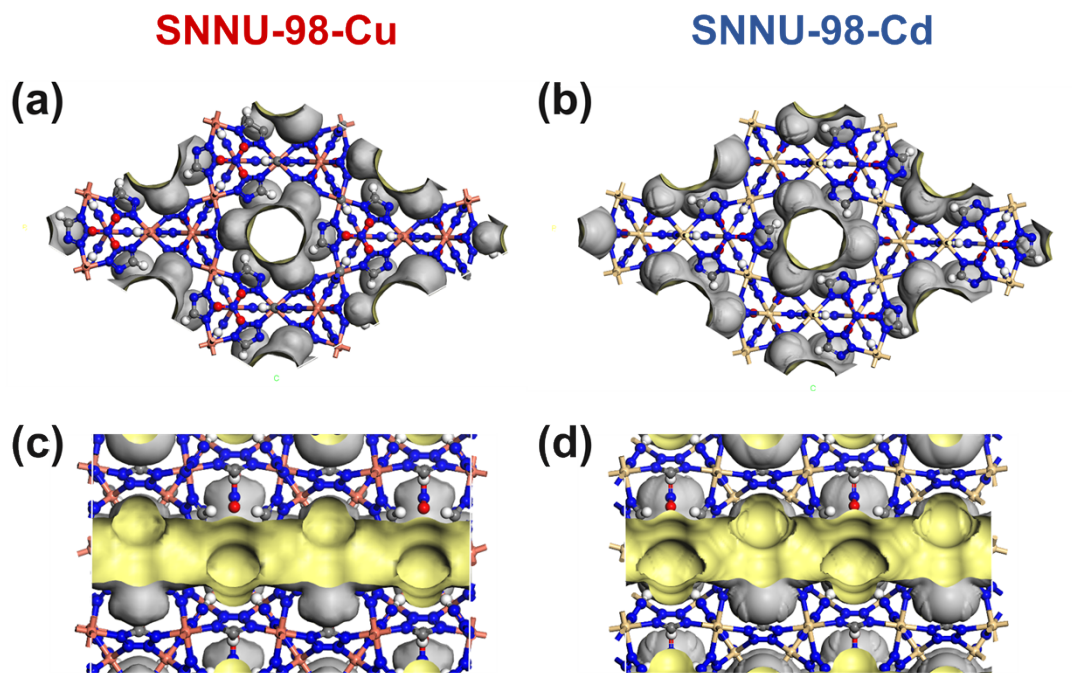


Figure S43. GCMC simulated density distributions in **SNNU-98-Cd** at 298 K and 1 bar of (a) CO_2/N_2 , (b) CO_2/CH_4 , (c) CH_4/N_2 , and (d) $\text{CO}_2/\text{CH}_4/\text{N}_2$.



	Occupied Volume (\AA^3)	Free Volume (\AA^3)	Surface Area (\AA^2)
SNNU-98-Cd	11681.18	4267.33	3494.25
SNNU-98-Cu	10239.30	3039.51	2733.52

Figure S44. The structure of **SNNU-98-Cd/Cu** (accessible Connolly surface obtained by using the Connolly radius of 1.8 Å and the Grid interval of 0.15 Å).

Table S1. Physical-chemical properties of CO₂, CH₄, N₂, CO and H₂.

Parameters	CO ₂	CH ₄	N ₂	CO	H ₂
Melting point (K)	216.55	90.6	63.14	68	13.8
Boiling point (K)	194.67	111.66	77.35	81.5	20.17
Critical temperature, T _c (K)	304.12	190.56	126.20	132.8	33.03
Critical pressure, P _c (MPa)	7.38	4.596	3.395	3.4	1.313
Polarizability (cm ³)	29.11×10^{25}	25.93×10^{25}	17.403×10^{25}	19.5×10^{25}	7.9×10^{25}
Quadrupole moment (esu cm ²)	4.30×10^{26}	0	1.52×10^{26}	2.7×10^{26}	0
Dimension (Å ³)	$3.19 \times 3.34 \times 5.36$	$3.8 \times 3.8 \times 3.8$	$2.99 \times 3.05 \times 4.05$	$3.8 \times 3.8 \times 4.3$	$2.9 \times 2.9 \times 3.1$
Kinetic Diameter (Å)	3.3	3.76	3.64	3.76	2.89

Table S2. Crystallographic data of SNNU-98-Cd.

Unit cell parameters	SNNU-98-Cd
Formula	C ₉ H ₂₃ Cd ₅ N ₃₇ O ₁₀
Formula weight	1371.64
Temperature/K	200.00
Crystal system	hexagonal
Space group	P6 ₃ /mmc
a/Å	13.0990(3)
b/Å	13.0990(3)
c/Å	13.4160(4)
α/°	90
β/°	90
γ/°	120
Volume/Å³	1993.56(11)
Z	2
ρ_{calc} g/cm³	2.285
μ/mm⁻¹	2.716
F(000)	1312.0
GOF	1.150
R_{int}	0.0342
R₁, wR₂ [I>=2σ (I)]	0.0752, 0.1903
R₁, wR₂ [all data]	0.0752, 0.1903
Largest diff. peak and hole (e A⁻³)	2.12/-4.00
CCDC number	2416690

Table S3. Comparison of pH stability of top-level MOFs and Cu-MOFs.

MOFs	Acid Stability	Basic Stability	pH Range of Stability	Duration	Reference
top-level highly-stable MOFs					
CPM-243	-1	15	16	48 h	²
SNNU-98-Cu	-0.5	13	13.5	7 days	This work
SNNU-98-Cu	1	12	11	6 months	This work
ZrPP-1	1	14.3	13.3	7 days	³
PFC-8	-1.1	12	13.1	/	⁴
UIO-66-NO₂	1	14	13	2 h	⁵
PCN-426-Cr	-0.6	12	12.6	12 h	⁶
Cr-MIL-142A	-0.5	12	12.5	/	⁷
BUT-8(Cr)	-1.1	11	12.1	1 week	⁸
MIL-101-Cr	0	12	12	2 months	¹
UIO-66-Zr	0	12	12	2 months	¹
Cr-SXU-1	-0.5	11	11.5	/	⁷
PCN-601	4	15.3	11.3	24 h	⁹
MOF-808	-1.1	10	11.1	24 h	¹⁰
Ni₃(BTP)₂	3	14	11	14 days	¹¹
PCN-333-Cr	0	11	11	24 h	¹²
JUC-1000	1.5	12.5	11	2 days	¹³
ZIF-8	4	14.9	10.9	24 h	¹⁴
PCN-224-Ni	1	11	10	24 h	¹⁵
NU-1000	1	11	10	/	¹⁶
MIL 53 (Al)	4	12	8	3 days	¹
Cu-MOFs					
SNNU-98-Cu	-0.5	13	13.5	7 days	This work
SNNU-98-Cu	1	12	11	6 months	This work
FJU-53-Cl	1	13	12	12 h	¹⁷
1-Cl	2	14	12	24 h	¹
JUC-1000	1.5	12.5	11	2 days	¹³
Cu-DMPHIDC	1	11	10	24 h	¹⁸
V-Cu-MOF	2	12	10	12 h	¹⁹
Cu-PSB	1	11	10	7 days	²⁰
FJI-H14	2	12	10	24 h	²¹
Cu-1	2	13	11	48 h	²²
Cu-BPEA-MOF	2	13	9	1 days	²³
CSMCRI-13	2	10	8	24 h	²⁴
USTC-6-Cu	2	10	8	7 days	²⁵
ZJNU-15	4	11	7	24 h	²⁶
BUT-155	4	10	6	24 h	²⁷

Table S4. The calculation details of Q_{st} for **SNNU-98-Cd**.

SNNU-98-Cd	CO ₂	CH ₄	N ₂
a0	-3032.09201	-3438.57902	-4290.24497
a1	-4623.90413	1192.21825	-5930.60662
a2	14874.71201	1819.88931	807075.8157
a3	-25669.35717	-17557.2131	-1.37239E7
a4	25092.21219	34900.4026	1.16771E8
a5	-14515.1942	-39858.72046	-5.6843E8
a6	4921.17168	26211.91485	1.57971E9
a7	-903.18249	-9213.30975	-2.32754E9
a8	69.2366	1339.42379	1.4088E9
c	273	273	273
b0	16.39116	18.34386	23.88658
b1	1.11637	-6.06308	-71.31154
b2	0.1967	10.55062	234.70559
c2	283	283	283
c3	298	298	298
Reduced Chi-Sqr	0.07003	0.00302	0.19926
Adj. R ²	0.97694	0.99664	0.92302

Table S5. The calculation details of Q_{st} for **SNNU-98-Cu**.

SNNU-98-Cu	CO ₂	CH ₄	N ₂
a0	-4157.98448	-2503.37918	-3116.08827
a1	600.74792	1502.98179	-43448.09551
a2	-31.54269	-5355.96879	2604236.72144
a3	-551.19722	14450.57111	-5.90228E7
a4	783.21763	-77747.82332	6.99162E8
a5	-582.78011	217423.25696	-4.73479E9
a6	242.21212	-323787.24877	1.83155E10
a7	-52.43954	244893.97865	-3.76027E10
a8	4.58	-74108.03307	3.175E10
c	273	273	273
b0	16.84223	15.47018	20.50073
b1	-1.27569	-4.40011	-47.45559
b2	0.72475	14.24341	296.3943
c2	283	283	283
c3	298	298	298
Reduced Chi-Sqr	6.83551E-4	6.3375E-4	0.03534
Adj. R ²	0.99972	0.9993	0.9823

Table S6. The fitting parameters for Langmuir-Freundlich (LF) isotherm model of **SNNU-98-Cd**.

SNNU-98-Cd		q	b	c	Reduced Chi-Sqr	R²
CO₂	273 K	3.52811	0.08216	0.87151	3.09826E-4	0.99957
	283 K	3.25177	0.04992	0.9354	1.00068E-4	0.9998
	298 K	2.93742	0.02537	1.00568	1.82497E-5	0.99996
CH₄	273 K	4.00152	0.00741	0.96605	1.81593E-6	0.99999
	283 K	3.16622	0.005	0.99408	1.38678E-6	0.99999
	298 K	2.39873	0.00385	1.02015	4.30389E-7	0.99999
N₂	273 K	20.05205	2.66488E-4	0.9401	3.26442E-6	0.99982
	283 K	1.19271	0.0021	1.08096	1.16067E-6	0.99988
	298 K	0.67317	0.00165	1.13522	2.2448E-6	0.99926

Table S7. The fitting parameters for Langmuir-Freundlich (LF) isotherm model of **SNNU-98-Cu**.

SNNU-98-Cu		q	b	c	Reduced Chi-Sqr	R²
CO₂	273 K	3.39058	0.28539	0.63526	8.33915E-4	0.99846
	283 K	3.12602	0.22548	0.22548	4.5945E-4	0.99915
	298 K	2.86176	0.13403	0.7907	1.51361E-4	3.6115E-8
CH₄	273 K	2.04491	0.00684	0.98731	1.137E-6	0.99998
	283 K	1.77718	0.00554	0.98705	5.7247E-7	0.99998
	298 K	1.73876	0.00384	0.98783	3.6115E-8	0.99999
N₂	273 K	2.32029	0.00138	1.00207	4.15078E-7	0.99995
	283 K	1.19858	0.00184	1.01386	3.94646E-7	0.99991
	298 K	0.74458	0.00178	1.01297	5.91226E-8	0.99996

Table S8. Summary of gas uptake, IAST selectivity and heat of adsorption data under different conditions for SNNU-98-Cd.

SNNU-98-Cd		CO ₂	CH ₄	N ₂
	273 K	149.7	80.1	20.6
Uptake (cm³ cm⁻³) at 1 bar	283 K	132.2	53.7	14.5
	298 K	109.1	37	8.4
	273 K		7.3	
CO₂/N₂ uptake ratio	283 K		9.1	
	298 K		13	
	273 K		1.9	
CO₂/CH₄ uptake ratio	283 K		2.5	
	298 K		2.9	
Q_{st} (kJ mol⁻¹)		25.2	28.6	35.7
	273 K		86.1-44.1	
IAST selectivity (15/85) of CO₂/N₂	273 K		69.9-70.4	
	298 K		55.9-70.1	
	273 K		12.5-7.7	
IAST selectivity (50/50) of CO₂/CH₄	283 K		11.5-9.3	
	298 K		7.9-8.5	
	273 K		5.9-5.8	
IAST selectivity (50/50) of CH₄/N₂	283 K		6.2-5.5	
	298 K		7.5-6.5	

Table S9. Summary of gas uptake, IAST selectivity and heat of adsorption data under different conditions for SNNU-98-Cu.

SNNU-98-Cu		CO ₂	CH ₄	N ₂
	273 K	149.4	41.6	14.8
Uptake (cm³ cm⁻³) at 1 bar	283 K	139.0	31.6	10.1
	298 K	124.1	24.0	6.2
	273 K		10.1	
CO₂/N₂ uptake ratio	283 K		13.8	
	298 K		20	
	273 K		3.6	
CO₂/CH₄ uptake ratio	283 K		4.4	
	298 K		5.2	
Q_{st} (kJ mol⁻¹)		34.6	20.8	25.9
	273 K		224.9-108	
IAST selectivity (15/85) of CO₂/N₂	283 K		810.8-1047.8	
	298 K		551.3-1509.3	
	273 K		168.1-152.4	
IAST selectivity (50/50) of CO₂/CH₄	283 K		142.7-172.7	
	298 K		90.3-94.6	
	273 K		4.5-4.1	
IAST selectivity (50/50) of CH₄/N₂	283 K		4.6-4.4	
	298 K		5.1-5.3	

Table S10. Summary of CO₂, CH₄ and N₂ adsorption and separation performance at 298 K for top-level MOF adsorbents sorted by the selectivity of CO₂/N₂ at 298 K and 1bar.

MOFs	Density (g cm ⁻³)	CO ₂ uptake at 1 bar (cm ³ cm ⁻³)	CH ₄ uptake at 1 bar (cm ³ cm ⁻³)	N ₂ uptake at 1 bar (cm ³ cm ⁻³)	-Q _{st} of CO ₂ (kJ mol ⁻¹)	Selectivity of CO ₂ /N ₂	Selectivity of CO ₂ /CH ₄	Ref
Qc-5-Cu-sql-β	1.492	72.2	2	0.3	36	40000 (293 K)	3300	²⁸
SIFSIX-3-Cu	1.605	92.8	/	6.8	54.0	15000	54	²⁹
Co-gallate	1.06	96.9	4.3	1.4	38	>10 ⁵	195	³⁰
Mg-gallate	1.06	119.9	4	1.4	37	>10 ⁴	2497	³⁰
Ni-gallate	1.06	92.8	4.3	1.2	39	>10 ⁴	3171	³⁰
ZU-36-Ni	1.82	106.4	7.7	6.1	55.5	4200	930	³¹
NKMOF-9a	1.876	87	5	4.2	69.6	1.6×10 ³	84000	³²
SNNU-98-Cu	2.292	124.1	24.0	6.2	34.6	1509.3	94.6	This work
ZU-301	1.744	95.3	25	7.8	38.9	846	111	³³
MUF-16	1.743	83.3	2.8	2.3	32	631	6690	³⁴
UTSA-120a	1.442	161.504	28.7	26.5	27	600 (296 K)	100	³⁵
NJU-Bai52	0.916	102.8	27.5	11.7	44.2	581	13.5	³⁶
ZJU-197	0.871	23.4	3.7	1.4	24.1	514.1	53	³⁷
ZU-66	1.544	157.7	7.3	2.8	35	355	136	³⁸
UTSA-16	1.659	160 (296 K)	21.2	1.6	34.6	314.7	~40	³⁹
CALF-20	1.763	156.8	/	14.6	39	230	/	⁴⁰
Mg-MOF-74	0.905	162.2	22.5	3.9	42	182.1	/	⁴¹
FJUT-3	1.247	62.3	/	6.1	41.7	178.3	/	⁴²
IIKGP-5	1.333	65.3	~17	~5.3	22.6	147.8 (295 K)	23.8	⁴³
FJI-H29	1.422	57.0	12.4	3.5	34	146	25	⁴⁴
ZnF(daTZ)	1.854	74.8	/	4.2	33	120	/	⁴⁵
SIFSIX-3-Zn	1.403	80.1	24.8	7.2	45	99.9	108	²⁹
UTSA-49	1.129	77.9	9	2.8	27	93.5	33.7	⁴⁶
[Co ₂ (4,4'-bpy)(L)]	1.280	46.6	14.6	4.6	29	70.5	9.9	⁴⁷
SIFSIX-2-Cu-i	1.246	150.7	13.1	4.2	31.9	70	/	^{29, 48}
SNNU-98-Cd	2.285	109.1	37	8.4	25.2	70.1	8.5	This work
NJU-Bai8	1.419	79.8	17.5	3.5	37.7	58.3	15.9	⁴⁹
JLU-MOF110(FeNi)	1.223	129	0.0	7.7	33.43	43.2	10.1	⁵⁰
PCN-88	0.657	59.9	12.4	1.9	35.0	15.0	7	⁵¹

Table S11. Summary of the CO₂/CH₄ (50/50) and CO₂/N₂(15/85) breakthrough performance with a total gas flow rate of 2 mL min⁻¹ at 298 K for top-level MOF CO₂ adsorbents sorted by the CO₂/N₂(15/85) separation interval times.

MOFs	Separation interval times of CO ₂ /CH ₄ (50/50) (min g ⁻¹)	Separation interval times of CO ₂ /N ₂ (15/85) (min g ⁻¹)	Ref
ZU-301	70	175	³³
FJI-H29	21	114	⁴⁴
SNNU-98-Cu	31.3	82.6	This work
UTSA-120a	35	80	³⁵
IITKGP-12	36	78	⁵²
SNNU-98-Cd	29	64.4	This work
Co-DOBDC-TPB	30	60 (50/50)	⁵³
Mg-gallate	-	59 (1.2 mL)	³⁰
FJUT-3	-	50	⁴²
JLU-MOF110(FeNi)	30.9	49.1	⁵⁰
Co-gallate	-	38 (1.2 mL)	³⁰
Mg-MOF-74	-	33	⁴¹
SIFSIX-2-Cu-i	3.3	33.3 (10/90)	⁴⁸
JLU-MOF110(Fe)	22.3	30.6 (50/50)	⁵⁰
ZU-66	28 min	28 min	³⁸
ZU-36-Ni	10	27	³¹
MUF-16	11 min	25 min	^{34, 54}
Ni-gallate	-	20 (1.2 mL)	³⁰
NKMOF-9a	13 min	20 min	³²
JLU-MOF110(In)	15.7	19.8 (50/50)	⁵⁰
ZnDatzBdc	10 (273 K)	10 (273 K)	⁴⁵
SIFSIX-3-Zn	6.7	5 (10/90)	²⁹

Table S12. Summary of the CO₂/CH₄/N₂ breakthrough performance at 298 K for top-level MOF CO₂ adsorbents.

MOFs	N ₂ breakthrough time (min g ⁻¹)	CH ₄ breakthrough time (min g ⁻¹)	CO ₂ breakthrough time (min g ⁻¹)	Flow rate	T (°C)	Concentration ratio	Ref
SNNU-98-Cu	9	18.3	80.9	5	298	5/5/90	This work
SNNU-98-Cd	12.9	22.4	47.9	5	298	5/5/90	This work
In-MOF-1	2.9	3	7.5	3	298	33/33/33	55
In-MOF-2	2	3	10	3	298	33/33/33	55
In-MOF-3	2	3	8	3	298	33/33/33	55
Run M1	0.1	0.1	100	/	313	20/20/20	56
Run M2	0.1	0.1	20	/	373	20/20/20	56
Run M3	0.1	0.1	5	/	423	20/20/20	56
Binder-Free Zeolite 4A	0.1	0.1	75	/	313	/	57
MOF-508b	20 s	25 s	40 s	/	323	/	58

Table S13. Breakthrough capacity of different components (from the breakthrough curve).

	Breakthrough capacity ($\text{cm}^3 \text{ cm}^{-3}$)		SNNU-98-Cd	SNNU-98-Cu
CO_2/N_2 (15/85) 2 mL min^{-1}	273 K	CO_2	84.3	94.8
	298 K	CO_2	56.9	64.6
CO_2/CH_4 (50/50) 2 mL min^{-1}	273 K	CO_2	132.5	106.3
	298 K	CO_2	131.1	97.4
$\text{CO}_2/\text{CH}_4/\text{N}_2$ (5/5/90) 5 mL min^{-1}	273 K	CO_2	47.4	60.3
	298 K	CO_2	28.7	41.5

Table S14. Gas adsorption capacity at different pressures (from the adsorption curve).

Adsorption capacity ($\text{cm}^3 \text{ cm}^{-3}$)	Pressure (bar)	SNNU-98-Cd	SNNU-98-Cu
273 K			
CO_2	0.05	49	76.8
CO_2	0.15	85.9	108
CO_2	0.5	127.6	134
298 K			
CO_2	0.05	21.2	52.3
CO_2	0.15	41.2	80
CO_2	0.5	85	109.5

References

- 1 K. Leus, T. Bogaerts, J. De Decker, H. Depauw, K. Hendrickx, H. Vrielinck, V. Van Speybroeck and P. Van Der Voort, *Microporous Mesoporous Mater.*, 2016, **226**, 110-116.
- 2 H. Yang, F. Peng, A. N. Hong, Y. Wang, X. Bu and P. Feng, *J. Am. Chem. Soc.*, 2021, **143**, 14470-14474.
- 3 E.-X. Chen, M. Qiu, Y.-F. Zhang, Y.-S. Zhu, L.-Y. Liu, Y.-Y. Sun, X. Bu, J. Zhang and Q. Lin, *Adv. Mater.*, 2018, **30**, 1704388.
- 4 G. Huang, L. Yang, Q. Yin, Z.-B. Fang, X.-J. Hu, A.-A. Zhang, J. Jiang, T.-F. Liu and R. Cao, *Angew. Chem. Int. Ed.*, 2020, **59**, 4385-4390.
- 5 M. Kandiah, M. H. Nilsen, S. Usseglio, S. Jakobsen, U. Olsbye, M. Tilset, C. Larabi, E. A. Quadrelli, F. Bonino and K. P. Lillerud, *Chem. Mater.*, 2010, **22**, 6632-6640.
- 6 T.-F. Liu, L. Zou, D. Feng, Y.-P. Chen, S. Fordham, X. Wang, Y. Liu and H.-C. Zhou, *J. Am. Chem. Soc.*, 2014, **136**, 7813-7816.
- 7 J.-H. Wang, Y. Zhang, M. Li, S. Yan, D. Li and X.-M. Zhang, *Angew. Chem. Int. Ed.*, 2017, **56**, 6478-6482.
- 8 A. J. Howarth, Y. Liu, P. Li, Z. Li, T. C. Wang, J. T. Hupp and O. K. Farha, *Nat. Rev. Mater.*, 2016, **1**, 15018.
- 9 K. Wang, X.-L. Lv, D. Feng, J. Li, S. Chen, J. Sun, L. Song, Y. Xie, J.-R. Li and H.-C. Zhou, *J. Am. Chem. Soc.*, 2016, **138**, 914-919.
- 10 W. Liang, H. Chevreau, F. Ragon, P. D. Southon, V. K. Peterson and D. M. D'Alessandro, *CrystEngComm*, 2014, **16**, 6530-6533.
- 11 V. Colombo, S. Galli, H. J. Choi, G. D. Han, A. Maspero, G. Palmisano, N. Masciocchi and J. R. Long, *Chem. Sci.*, 2011, **2**, 1311.
- 12 X. Lian, D. Feng, Y.-P. Chen, T.-F. Liu, X. Wang and H.-C. Zhou, *Chem. Sci.*, 2015, **6**, 7044-7048.
- 13 H. He, Q. Sun, W. Gao, J. A. Perman, F. Sun, G. Zhu, B. Aguila, K. Forrest, B. Space and S. Ma, *Angew. Chem. Int. Ed.*, 2018, **57**, 4657-4662.
- 14 K. S. Park, Z. Ni, A. P. Côté, J. Y. Choi, R. Huang, F. J. Uribe-Romo, H. K. Chae, M. O'Keeffe and O. M. Yaghi, *Proceedings of the National Academy of Sciences*, 2006, **103**, 10186-10191.
- 15 D. Feng, W.-C. Chung, Z. Wei, Z.-Y. Gu, H.-L. Jiang, Y.-P. Chen, D. J. Daresbourg and H.-C. Zhou, *J. Am. Chem. Soc.*, 2013, **135**, 17105-17110.
- 16 F. Yang, G. Xu, Y. Dou, B. Wang, H. Zhang, H. Wu, W. Zhou, J.-R. Li and B. Chen, *Nat. Energy*, 2017, **2**, 877-883.
- 17 L. Wang, Y. Ye, Z. Li, Q. Lin, J. Ouyang, L. Liu, Z. Zhang and S. Xiang, *Cryst. Growth Des.*, 2017, **17**, 2081-2089.
- 18 W. Chen, C. Yang, S. Yu, Z. Li and G. Li, *Polyhedron*, 2019, **158**, 377-385.
- 19 H.-R. Tian, Z. Zhang, S.-M. Liu, T.-Y. Dang, Z. Li, Y. Lu and S.-X. Liu, *Green Chem.*, 2020, **22**, 7513-7520.
- 20 S. Chand Pal, R. Krishna and M. C. Das, *Chem. Eng. J.*, 2023, **460**, 141795.
- 21 L. Liang, C. Liu, F. Jiang, Q. Chen, L. Zhang, H. Xue, H.-L. Jiang, J. Qian, D. Yuan and M. Hong, *Nat. Commun.*, 2017, **8**, 1233.
- 22 Z. L. Ma, P. X. Liu, Z. Y. Liu, J. J. Wang, L. B. Li and L. Tian, *Inorg. Chem.*, 2021, **60**, 6550-6558.
- 23 D.-M. Chen, C.-X. Sun, C.-S. Liu and M. Du, *Inorg. Chem.*, 2018, **57**, 7975-7981.
- 24 N. Seal and S. Neogi, *ACS Appl. Mater. Interfaces*, 2021, **13**, 55123-55135.
- 25 Z.-R. Jiang, J. Ge, Y.-X. Zhou, Z. U. Wang, D. Chen, S.-H. Yu and H.-L. Jiang, *NPG Asia Mater.*, 2016, **8**, e253.
- 26 Z. Jiang, Y. Zou, T. Xu, L. Fan, P. Zhou and Y. He, *Dalton Trans.*, 2020, **49**, 3553-3561.
- 27 Y. Chen, B. Wang, X. Wang, L.-H. Xie, J. Li, Y. Xie and J.-R. Li, *ACS Appl. Mater. Interfaces*, 2017, **9**, 27027-27035.
- 28 K.-J. Chen, D. G. Madden, T. Pham, K. A. Forrest, A. Kumar, Q.-Y. Yang, W. Xue, B. Space, J. J. Perry, J.-P. Zhang, X.-M. Chen and M. J. Zaworotko, *Angew. Chem. Int. Ed.*, 2016, **55**, 10268-10272.
- 29 O. Shekhah, Y. Belmabkhout, Z. Chen, V. Guillerm, A. Cairns, K. Adil and M. Eddaoudi, *Nat. Commun.*, 2014, **5**, 4228.
- 30 F. Chen, J. Wang, L. Guo, X. Huang, Z. Zhang, Q. Yang, Y. Yang, Q. Ren and Z. Bao, *Sep. Purif. Technol.*, 2022, **292**, 121031.
- 31 Z. Zhang, Q. Ding, S. B. Peh, D. Zhao, J. Cui, X. Cui and H. Xing, *Chem. Commun.*, 2020, **56**, 7726-7729.
- 32 S. Geng, H. Xu, C.-S. Cao, T. Pham, B. Zhao and Z. Zhang, *Angew. Chem. Int. Ed.*, 2023, **62**, e202305390.
- 33 C. Yu, Q. Ding, J. Hu, Q. Wang, X. Cui and H. Xing, *Chem. Eng. J.*, 2021, **405**, 126937.
- 34 O. T. Qazvini and S. G. Telfer, *ACS Appl. Mater. Interfaces*, 2021, **13**, 12141-12148.
- 35 H.-M. Wen, C. Liao, L. Li, A. Alsalme, Z. Alothman, R. Krishna, H. Wu, W. Zhou, J. Hu and B. Chen, *J. Mater. Chem. A*, 2019, **7**, 3128-3134.
- 36 X. Song, M. Zhang, C. Chen, J. Duan, W. Zhang, Y. Pan and J. Bai, *J. Am. Chem. Soc.*, 2019, **141**, 14539-14543.
- 37 L. Zhang, K. Jiang, Y. Yang, Y. Cui, B. Chen and G. Qian, *J. Solid State Chem.*, 2017, **255**, 102-107.
- 38 L. Yang, X. Cui, Y. Zhang, Q. Wang, Z. Zhang, X. Suo and H. Xing, *ACS Sustain. Chem. Eng.*, 2019, **7**, 3138-3144.
- 39 S. Xiang, Y. He, Z. Zhang, H. Wu, W. Zhou, R. Krishna and B. Chen, *Nat. Commun.*, 2012, **3**, 954.
- 40 J.-B. Lin, T. T. T. Nguyen, R. Vaidhyanathan, J. Burner, J. M. Taylor, H. Durekova, F. Akhtar, R. K. Mah, O. Ghaffari-Nik, S. Marx, N. Fylstra, S. S. Iremonger, K. W. Dawson, P. Sarkar, P. Hovington, A. Rajendran, T. K. Woo and G. K. H. Shimizu, *Science*, 2021, **374**, 1464-1469.
- 41 S. R. Caskey, A. G. Wong-Foy and A. J. Matzger, *J. Am. Chem. Soc.*, 2008, **130**, 10870-10871.
- 42 L. Zhang, Z. He, Y. Liu, J. You, L. Lin, J. Jia, S. Chen, N. Hua, L.-A. Ma, X. Ye, Y. Liu, C.-X. Chen and Q. Wang, *ACS Appl. Mater. Interfaces*, 2023, **15**, 30394-30401.
- 43 A. Pal, S. Chand, S. M. Elahi and M. C. Das, *Dalton Trans.*, 2017, **46**, 15280-15286.
- 44 D. Wu, C. Liu, J. Tian, F. Jiang, D. Yuan, Q. Chen and M. Hong, *Inorg. Chem.*, 2020, **59**, 13542-13550.
- 45 Z. Shi, Y. Tao, J. Wu, C. Zhang, H. He, L. Long, Y. Lee, T. Li and Y.-B. Zhang, *J. Am. Chem. Soc.*, 2020, **142**, 2750-2754.

- 46 S. Xiong, Y. Gong, H. Wang, H. Wang, Q. Liu, M. Gu, X. Wang, B. Chen and Z. Wang, *Chem. Commun.*, 2014, **50**, 12101-12104.
- 47 V. G. a. S. K. Mandal, *Dalton Trans.*, 2019, **48**, 415-425.
- 48 P. Nugent, Y. Belmabkhout, S. D. Burd, A. J. Cairns, R. Luebke, K. Forrest, T. Pham, S. Ma, B. Space, L. Wojtas, M. Eddaoudi and M. J. Zaworotko, *Nature*, 2013, **495**, 80-84.
- 49 L. Du, Z. Lu, K. Zheng, J. Wang, X. Zheng, Y. Pan, X. You and J. Bai, *J. Am. Chem. Soc.*, 2013, **135**, 562-565.
- 50 W. Li, X. Liu, X. Yu, B. Zhang, C. Ji, Z. Shi, L. Zhang and Y. Liu, *Inorg. Chem.*, 2023, **62**, 18248-18256.
- 51 J.-R. Li, J. Yu, W. Lu, L.-B. Sun, J. Sculley, P. B. Balbuena and H.-C. Zhou, *Nat. Commun.*, 2013, **4**, 1538.
- 52 A. Pal, S. Chand, D. G. Madden, D. Franz, L. Ritter, B. Space, T. Curtin, S. Chand Pal and M. C. Das, *ACS Appl. Mater. Interfaces*, 2020, **12**, 41177-41184.
- 53 H. Xu, J. Li, L. Liu, F.-S. Liang and Z.-B. Han, *Inorg. Chem.*, 2023, **62**, 13530-13536.
- 54 O. T. Qazvini, R. Babarao and S. G. Telfer, *Nat. Commun.*, 2021, **12**, 197.
- 55 Y.-Q. Zhang, L. Liu, W.-Z. Li, B.-H. Wu, C.-N. Li, J.-Q. Chu and Z.-B. Han, *Inorg. Chem.*, 2024, **63**, 7705-7713.
- 56 L. F. A. S. Zafanelli, A. Henrique, M. Karimi, A. E. Rodrigues and J. A. C. Silva, *Ind. Eng. Chem. Res.*, 2020, **59**, 13724-13734.
- 57 E. Aly, L. F. A. S. Zafanelli, A. Henrique, M. Golini Pires, A. E. Rodrigues, K. Gleichmann and J. A. C. Silva, *Ind. Eng. Chem. Res.*, 2021, **60**, 15236-15247.
- 58 L. Bastin, P. S. Bárcia, E. J. Hurtado, J. A. C. Silva, A. E. Rodrigues and B. Chen, *J. Phys. Chem. C*, 2008, **112**, 1575-1581.